Biomechan Model Mechanobiol (2005) 4: 100–117
DOI 10.1007/s10237-005-0069-8

ORIGINAL PAPER

Alan D. Freed · Daniel R. Einstein · Ivan Vesely

Invariant formulation for dispersed transverse isotropy in aortic heart valves

An efficient means for modeling fiber splay

Received: 27 April 2004 / Accepted: 2 December 2004 / Published online: 27 August 2005
© Springer-Verlag Berlin Heidelberg 2005

Abstract Most soft tissues possess an oriented architecture of collagen fiber bundles, conferring both anisotropy and nonlinearity to their elastic behavior. Transverse isotropy has often been assumed for a subset of these tissues that have a single macroscopically-identifiable preferred fiber direction. Micro-structural studies, however, suggest that, in some tissues, collagen fibers are approximately normally distributed about a mean preferred fiber direction. Structural constitutive equations that account for this dispersion of fibers have been shown to capture the mechanical complexity of these tissues quite well. Such descriptions, however, are computationally cumbersome for two-dimensional (2D) fiber distributions, let alone for fully three-dimensional (3D) fiber populations. In this paper, we develop a new constitutive law for such tissues, based on a novel invariant theory for dispersed transverse isotropy. The invariant theory is derived from a novel closed-form 'splay invariant' that can easily handle 3D fiber populations, and that only requires a single parameter in the 2D case. The model fits biaxial data for aortic valve tissue as accurately as the standard structural model. Modification of the fiber stress–strain law requires no reformulation of the constitutive tangent matrix, making the model flexible for different types of soft tissues. Most importantly, the model is computationally expedient in a finite-element analysis, demonstrated by modeling a bioprosthetic heart valve.

1 Introduction

Constitutive modeling of soft tissues is an important prerequisite for the computational analysis of the systems-level response of biological structures to applied loads and pressures. Computational modeling in many cases is the only way, short of implantation, to evaluate the mechanical response of tissues to the full 3D mechanical environment seen in vivo. Moreover, computational modeling permits the analyst to directly query the relationship between structure and stress, and to explore the design space of newly proposed implants, bioprostheses or tissue-engineered constructs. Numerical models of tissue systems can be computationally intensive. This is particularly true of tissues that require complex material models, and systems that involve fluid–structure interactions. The material models used in these systems must not only be accurate, they must also be computationally efficient.

The past few years have seen an increased interest in nonlinear continuum mechanics as a framework for describing the mechanical behavior of soft tissues. The now well-established mathematics of this field provides a perspective from which rigorous, thermodynamically-reasonable constitutive equations can be proposed—a characteristic that was lacking in many earlier ad hoc tissue descriptions. The geometric and material nonlinearities seen in tissues fit well into this framework, and anisotropy is readily handled by the theory of invariants (Spencer 1972). In addition, constitutive equations posed within this

---

A. D. Freed
Bio Science and Technology Branch, MS 49-3,
NASA's John H. Glenn Research Center at Lewis Field,
21000 Brookpark Road, Cleveland, OH 44135, USA

A. D. Freed (✉)
Department of Biomedical Engineering, ND-20,
The Cleveland Clinic Foundation, 9500 Euclid Avenue,
Cleveland, OH 44195, USA
E-mail: Alan.D.Freed@nasa.gov

D. R. Einstein
Environmental Molecular Sciences Laboratory, MS P7-56,
Pacific Northwest National Laboratory, 790 Sixth Street,
Richland, WA 99354, USA
E-mail: Daniel.Einstein@pnl.gov

I. Vesely
Cardiothoracic Surgery Research, Saban Research Institute,
MS 66, Children's Hospital Los Angeles,
4650 Sunset Boulevard, Los Angeles, CA 90027, USA
E-mail: IVesely@chla.usc.edu

framework can call upon developed computational techniques, permitting the exploration of tissue-level and organ-level mechanics involving finite deformations. An excellent reference for both nonlinear continuum mechanics and related variational principles, as they apply to soft tissues, is the textbook by Holzapfel (2000).

Structural constitutive equations that view soft tissues as statistically-oriented distributions of fibers come from a different tradition based on the experimental observation of fiber dispersion, or splay. For example, Sacks (2003) showed a correlation between the intensity distribution of the small-angle light scattering of bovine pericardium and both fiber orientation and dispersion. Similarly, Holzapfel et al.(2002) showed that smooth muscle cells in arterial media are statistically oriented around two opposing helical directions. From these cellular orientations, collagen fiber orientations were inferred. An earlier observation of fiber dispersal in bovine pericardium was documented by Zioupos and Barbenel (1994). The need to account for fiber dispersion architectures when modeling soft tissues was first addressed by Lanir (1983). Since then, structural models with dispersion have been proposed for passive myocardium (Horowitz et al. 1988), lung (Mijailovich et al. 1993), heart valves (Sacks 2000), aorta (Wuyts et al. 1995), and tendon and ligament (Hurschler et al. 1997). To model fiber splay, both the von Mises (Hurschler et al. 1997) and Gaussian (Sacks 2000) distributions have been adopted.

Mathematically, the inclusion of such probability distribution functions into constitutive models presents little challenge, but computationally, they are cumbersome. The probability density function acts as a weighting function in the fiber stress–strain rule. Functionally, in the 2D case, this can be represented as

$$\mathrm{S} + p\mathrm{C}^{-1} = \int_{-\pi/2}^{\pi/2} S_f(\theta, \mathrm{C}) R(\theta) \mathbf{a}_0 \otimes \mathbf{a}_0(\theta) \mathrm{d}\theta, \tag{1}$$

where S is the second Piola-Kirchhoff stress, C is the Lagrangian metric, p is a Lagrange multiplier to force the constraint of incompressibility, S_f (θ, C) is a fiber stress–strain rule, R(θ) is a probability distribution function, and $\mathbf{a}_0 \otimes \mathbf{a}_0(\theta)$ governs the orientation of a fiber family in the 2D plane. What is important to note is that the product of fiber stress and the weighting function must be integrated over a full semi-circle in the 2D case, Eq. 1, or an equivalent hemisphere in the 3D case. These integrals have traditionally been evaluated numerically. Numerical experiments on one such equation for mitral-valve tissue suggested that 18 discrete intervals were necessary to capture the full range of constitutive behavior (Einstein 2002). This is mechanically equivalent to having 18 weighted fibers in the plane. A single integral of this kind in the constitutive equation implies that two integrals need to be evaluated in the constitutive tangent matrix. Likewise, 3D fiber dispersion would require two integrals to be evaluated for stress, and four for the constitutive tangent matrix. In the computational model, these operations are evaluated at every iteration, of every time step, at every Gauss point, for every finite element, in some geometric model of interest.

In this paper, we develop an alternative constitutive construction for tissues whose collagen fiber populations are statistically distributed. To address the problem of computational cost, the integral in Eq. 1 is replaced with a novel closed-form ‘splay invariant’ that requires a single parameter in the 2D case, and a single operation per iteration. To evaluate the model, we compare its correlative capability against published biaxial data for aortic valve tissue. In addition, we compare the capabilities of our model against those of a published structural model (Billiar and Sacks 2000b; Einstein 2002) based on the paradigm in Eq. 1 and which fits the data quite well.

2 Theory

Select a rectangular Cartesian coordinate system described by a set of orthonormal base vectors $\{\mathbf{e}_1, \mathbf{e}_2, \mathbf{e}_3\}$. Consider a mass point originally given by the set of coordinates $\mathbf{X} = (X_1, X_2, X_3)$ assigned at an arbitrary reference time of t_0. At current time t, this mass element is located by a different set of coordinates $\mathbf{x} = (x_1, x_2, x_3)$. Let the motion of this mass point through space be described by a one-parameter family (in time) of locations considered to be continuous and sufficiently differentiable to allow for the definition of a deformation gradient tensor

$$\mathrm{F}(t_0, t) = F_{ij}(t_0, t)\mathbf{e}_i \otimes \mathbf{e}_j \text{ with components}$$

$$F_{ij}(t_0, t) = \frac{\partial x_i}{\partial X_j}, \tag{2}$$

where ⊗ is the dyadic vector product, and indices i and j have values 1, 2, 3. The ability to invert this field, guaranteed by the conservation of mass, (i.e., $\mathrm{F}^{-1}(t_0, t) = F_{ij}^{-1}(t_0, t)\mathbf{e}_i \otimes \mathbf{e}_j$ with components $F_{ij}^{-1}(t_0, t) = \partial X_i / \partial x_j$ and characteristic $\mathrm{F}^{-1}\mathrm{F} = \mathrm{F}\mathrm{F}^{-1} = \mathrm{I}$, where I is the identity tensor) ensures that a given particle cannot occupy two locations at the same instant of time, and that two discrete particles cannot occupy a single location at any moment of time.

Affiliated with the deformation gradient tensor defined in Eq. 2 are the left- and right-deformation tensors [1] defined by

---

[1] Tensors $\mathrm{B} = \mathrm{F}\mathrm{F}^{\mathrm{T}} = \mathrm{V}^2$ and $\mathrm{C} = \mathrm{F}^{\mathrm{T}}\mathrm{F} = \mathrm{U}^2$ are often referred to as the left and right Cauchy–Green deformation tensors, respectively, because V and U are called the left- and right-stretch tensors, so named because of the polar decomposition $\mathrm{F} = \mathrm{V}\mathrm{R} = \mathrm{R}\mathrm{U}$ wherein $\mathrm{R}\mathrm{R}^{\mathrm{T}} = \mathrm{I}$. We prefer to call B and C the left- and right-deformation tensors. Historically, Cauchy (1827, pp 60–69), used B^{-1} (sometimes expressed as c) and Green (1841) used C, while Finger (1894) introduced their duals, B (sometimes expressed as b) and C^{-1}. Therefore, naming these fields after Cauchy and Green seems an injustice to Finger, especially since Finger introduced B into the literature.

$$\mathrm{B} = \mathrm{F}\mathrm{F}^{\mathrm{T}} \quad \text{and} \quad \mathrm{C} = \mathrm{F}^{\mathrm{T}}\mathrm{F} \tag{3}$$

respectively, where ‘T’ implies transpose (e.g., $B_{ij} = F_{ik}F_{jk}$ and $C_{ij} = F_{ki}F_{kj}$ with the repeated index k being summed from 1 to 3 in the usual manner). Inverses B^{-1} and C^{-1} exist because the tensor fields B and C are symmetric positive-definite. The left-deformation tensor $\mathrm{B}(\mathbf{x}; t_0, t) = B_{ij}(\mathbf{x}; t_0, t)\mathbf{e}_i \otimes \mathbf{e}_j$ appears in Eulerian constructions, while the right-deformation tensor $\mathrm{C}(\mathbf{X}; t_0, t) = C_{ij}(\mathbf{X}; t_0, t)\mathbf{e}_i \otimes \mathbf{e}_j$ appears in Lagrangian constructions.

2.1 Invariants

Consider a vector $\mathbf{a}_0(\mathbf{X}; t_0) = a_{0i}(\mathbf{X}; t_0)\mathbf{e}_i$ of length $\mathbf{a}_0 \cdot \mathbf{a}_0 = a_{0k}a_{0k} = 1$ that lies tangent to a material line of strength (e.g., a fiber) in the reference state t_0. After a deformation, this material line will have stretched by an amount λ (t_0,t) that is quantified by $\lambda^2 = \mathbf{a}_0 \cdot \mathrm{C}\mathbf{a}_0 = a_{0k}C_{k\ell}a_{0\ell}$. As such, there exists a spatial vector $\mathbf{a}(\mathbf{x}; t_0, t) = a_i(\mathbf{x}; t_0, t)\mathbf{e}_i$ with L_2 norm $\| \mathbf{a} \|_2 = \sqrt{\mathbf{a} \cdot \mathbf{a}} = \lambda$ that in the deformed state t of Green's metric C relates to material vector $\mathbf{a}_0$ via the mapping $\mathbf{a} = \mathrm{F}\,\mathbf{a}_0$.

From the classic theory of invariants (Spencer 1972), there are five invariants that are needed to describe a material with transverse isotropy (i.e., a material with a single fiber family); they are:

$$\begin{aligned} &I_{\mathrm{I}} = \mathrm{tr}\mathrm{C}, \quad I_{\mathrm{II}} = \frac{1}{2}((\mathrm{tr}\ \mathrm{C})^2 - \mathrm{tr}(\mathrm{C}^2)), \\ &\quad I_{\mathrm{III}} = \det \mathrm{C} = (\det\ \mathrm{F})^2, \end{aligned} \tag{4}$$

$$I_{\mathrm{IV}} = \mathbf{a}_0 \cdot \mathrm{C}\mathbf{a}_0 = \mathbf{a} \cdot \mathbf{a} = \lambda^2, \quad I_{\mathrm{V}} = \mathbf{a}_0 \cdot \mathrm{C}^2\mathbf{a}_0 = \mathbf{a} \cdot \mathrm{B}\mathbf{a}, \tag{5}$$

where $\mathrm{tr}\ \mathrm{C} = C_{kk}$ is the trace of C, and $\det \mathrm{C} = \frac{1}{3}\left\{\mathrm{tr}\mathrm{C}^3 - \mathrm{tr}\ \mathrm{C}[(\mathrm{tr}\ \mathrm{C})^2 - 3\mathrm{tr}\ \mathrm{C}^2]\right\}$ denotes its determinant. The three invariants in Eq. 4 account for isotropic effects, while the two invariants in Eq. 5 account for anisotropic effects.

Invariants I_{IV} and I_{V} idealize all fibers in a family as being parallel, which is not indicative of soft biological tissues. The fiber architectures of soft tissues are splayed. We, therefore, seek an alternative pair of invariants—call them $I_{\langle\mathrm{IV}\rangle}$ and $I_{\langle\mathrm{V}\rangle}$—that can replace I_{IV} and I_{V} for dispersed fiber architectures, yet analytically reduce to I_{IV} and I_{V} in the absence of fiber dispersion. It is sufficient to define these new invariants as

$$I_{\langle\mathrm{IV}\rangle} = \mathrm{tr}(\mathrm{F}\mathrm{K}\mathrm{F}^{\mathrm{T}}) = \mathrm{tr}(\mathrm{K}\mathrm{C}) \quad \text{and} \quad I_{\langle\mathrm{V}\rangle} = \mathrm{tr}(\mathrm{C}\mathrm{K}\mathrm{C}), \tag{6}$$

where $\mathrm{K}(\mathbf{X}) = K_{ij}(\mathbf{X})\mathbf{e}_i \otimes \mathbf{e}_j$ is constrained so that $\mathrm{K} \to \mathbf{a}_0 \otimes \mathbf{a}_0$ in the absence of splay. Tensor K is a material constant. The main objective of this paper is to derive such a K appropriate for describing the anisotropy caused by fiber dispersion.

2.2 Elasticity

The strain-energy density per unit mass, when written in the Lagrangian frame, is given by (Lodge 1974, pp 194–195)

$$\mathrm{d}W = \frac{1}{2\varrho_0}\mathrm{tr}(\mathrm{S}\ \mathrm{d}\mathrm{C}), \tag{7}$$

where $\mathrm{d}W(\mathbf{X}; t_0, t, \mathrm{d}t)$ represents the work done on a material element of mass density $\varrho = \varrho(\mathbf{x}; t)$, with $\varrho_0 = \varrho(\mathbf{X}; t_0)$. Work is caused by an imposed displacement acting on the mass element, manifested here as the strain increment $\frac{1}{2}\mathrm{d}\mathrm{C}(\mathbf{X}; t_0, t, \mathrm{d}t)$.The material responds to this displacement through the creation of forces, thereby producing a state of stress $\mathrm{S}(\mathbf{X};\ t_0,\ \mathrm{t})$.

The second Piola-Kirchhoff stress tensor S pushes forward into the Eulerian frame (Holzapfel 2000, pp 82–84) becoming the Cauchy stress tensor $\mathrm{T}(\mathbf{x};\mathrm{t})$ via the well-known mapping $\mathrm{T} = (\varrho/\varrho_0)\mathrm{F}\mathrm{S}\mathrm{F}^{\mathrm{T}}$. Formula $\varrho/\varrho_0 = \det \mathrm{F}$ follows from the conservation of mass. Green strain $\mathrm{E}\ (\mathbf{X};\ t_0,\ \mathrm{t})$, defined by $\mathrm{E} = (1/2)(\mathrm{C} - 1)$, has an incremental change $\mathrm{dE}\ (\mathbf{X}; t_0,\mathrm{t},\mathrm{dt})$ of $\mathrm{dE} = (1/2)\mathrm{dC} = \mathrm{F}^{\mathrm{T}}\hat{\mathrm{E}}\mathrm{F}$, wherein $\mathrm{F}(t_0,t)$ and $\hat{E}(\mathbf{x}; t, t + \mathrm{d}t) = (1/2)(\hat{C} - I)$ with $\hat{C}(\mathbf{x}; t, t + \mathrm{d}t) = \hat{F}^{\mathrm{T}}\hat{F}$ given $\hat{F}_{ij}(t, t + \mathrm{d}t) = \partial x_i(t + \mathrm{d}t)/\partial x_j(t)$ where $\hat{\mathrm{F}}(t, t + \mathrm{d}t) = \hat{F}_{ij}(t, t + \mathrm{d}t)\mathbf{e}_i \otimes \mathbf{e}_j$, with dE appearing in $\varrho_0\mathrm{d}W = \mathrm{tr}(\mathrm{S}\ \mathrm{dE})$.

An elastic solid is defined by the constitutive law (Leonov 2000)

$$\mathrm{S} = 2\varrho_0\frac{\partial W(T, \mathrm{C})}{\partial \mathrm{C}}, \tag{8}$$

with an isochoric constraint of $\det \mathrm{F} = 1$ also applying whenever the material is incompressible. Thermodynamics requires W to be a function of both temperature T and deformation C. Because the human body maintains a nearly isothermal state, the temperature dependence of tissues is usually neglected in their analysis. The strain-energy density W will also depend on any number of material constants that may appear as scalar, vector or tensor fields.

Adopting the invariants in Eqs. 4 and 6 as our integrity basis, the general constitutive equation for a transversely isotropic elastic solid with splay, when expressed in the Lagrangian frame, yields the constitutive equation[2]

$$\begin{aligned} \mathrm{S} = {} & \left(\mathcal{W}_{,\mathrm{I}} + I_{\mathrm{I}}\mathcal{W}_{,\mathrm{II}}\right)I - \mathcal{W}_{,\mathrm{II}}\mathrm{C} + I_{\mathrm{III}}\mathcal{W}_{,\mathrm{III}}\mathrm{C}^{-1} \\ & + \mathcal{W}_{,\langle\mathrm{IV}\rangle}\mathrm{K} + \mathcal{W}_{,\langle\mathrm{V}\rangle}(\mathrm{C}\mathrm{K} + \mathrm{K}\mathrm{C}), \end{aligned} \tag{9}$$

that, when pushed forward into the Eulerian frame, becomes

---

[2] The following well-known tensor derivatives are useful in the derivation of constitutive formulae:
$\frac{\partial\,\mathrm{tr}\ \mathrm{Z}}{\partial \mathrm{Z}} = 1, \quad \frac{\partial\,\mathrm{tr}\ \mathrm{Z}^{-1}}{\partial \mathrm{Z}} = -\mathrm{Z}^{-\mathrm{T}}\mathrm{Z}^{-\mathrm{T}}, \frac{\partial \det \mathrm{Z}}{\partial \mathrm{Z}} = \det(\mathrm{Z})\mathrm{Z}^{-\mathrm{T}},$
$\det \mathrm{Z} \neq 0.$

$$\tau = (\mathcal{W}_{,\mathrm{I}} + I_{\mathrm{I}}\mathcal{W}_{,\mathrm{II}})\mathrm{B} - \mathcal{W}_{,\mathrm{II}}\mathrm{B}^2 + I_{,\mathrm{III}}\mathcal{W}_{,\mathrm{III}}\mathrm{1} + \mathcal{W}_{,\langle\mathrm{IV}\rangle}\mathrm{A} + \mathcal{W}_{,\langle\mathrm{V}\rangle}(\mathrm{BA} + \mathrm{AB}),$$

where in $\mathcal{W}_{,\mathrm{I}} = 2\varrho_0 \partial W/\partial I_{\mathrm{I}}$, etc., and $\mathrm{A}(\mathbf{x}; t_0, t) = \mathrm{FKF}^{\mathrm{T}}$. Tensor $\tau(\mathbf{x}; t_0, t) = (\varrho_0/\varrho)\mathrm{T}$ is known as the Kirchhoff stress tensor.

It is a straightforward matter to extend any, existing, transversely isotropic, integrity basis (e.g., Criscione et al. 2001) into an equivalent basis that accounts for splay by applying an appropriate mapping. For example, if the classic integrity basis $\{I_{\mathrm{I}}, I_{\mathrm{II}}, I_{\mathrm{III}}, I_{\mathrm{IV}}, I_{\mathrm{V}}\}$ maps into some other basis $\{\beta_{\mathrm{I}}, \beta_{\mathrm{II}}, \beta_{\mathrm{III}}, \beta_{\mathrm{IV}}, \beta_{\mathrm{V}}\}$ by a known mapping, then using $\{I_{\mathrm{I}}, I_{\mathrm{II}}, I_{\mathrm{III}}, I_{\langle\mathrm{IV}\rangle}, I_{\langle\mathrm{V}\rangle}\}$ in place of $\{I_{\mathrm{I}}, I_{\mathrm{II}}, I_{\mathrm{III}}, I_{\mathrm{IV}}, I_{\mathrm{V}}\}$ will produce $\{\beta_{\langle\mathrm{I}\rangle}, \beta_{\langle\mathrm{II}\rangle}, \beta_{\langle\mathrm{III}\rangle}, \beta_{\langle\mathrm{IV}\rangle}, \beta_{\langle\mathrm{V}\rangle}\}$ for its splay invariants.

The challenges that lie ahead are: (1) to establish a tensor field K that is appropriate for splayed fiber architectures, and (2) to arrive at a simple set of five scalar-valued gradients $\{\mathcal{W}_{,\mathrm{I}}, \mathcal{W}_{,\mathrm{II}}, \mathcal{W}_{,\mathrm{III}}, \mathcal{W}_{,\langle\mathrm{IV}\rangle}, \mathcal{W}_{,\langle\mathrm{V}\rangle}\}$ that allows Eqs. 9, 10 to aptly describe some known set of experimental data.

3 Anisotropic stiffness

For the purpose of assessing the effect of fiber orientation on stiffness, it is useful to switch from the global coordinate system (1, 2, 3) with base vectors $\{\mathbf{e}_1, \mathbf{e}_2, \mathbf{e}_3\}$ to a local or intrinsic coordinate system (α, β, γ) with base vectors $\{\mathbf{e}_\alpha, \mathbf{e}_\beta, \mathbf{e}_\gamma\}$. These local coordinates are selected so that the unit vector in the α-direction (i.e., $\mathbf{e}_\alpha$) lies coaxial with the mean direction of fiber orientation $\mathbf{a}_0$, while the unit vectors in the β- and γ-directions lie in the transverse plane. Because both the intrinsic and global coordinate systems are considered to be rectangular Cartesian, there exists an unique, orthogonal, rotation matrix Q such that

$$\mathbf{e}_1 = \mathrm{Q}\mathbf{e}_\alpha, \quad \mathbf{e}_2 = \mathrm{Q}\mathbf{e}_\beta, \quad \mathbf{e}_3 = \mathrm{Q}\mathbf{e}_\gamma, \tag{11}$$

where $\mathrm{Q}^{\mathrm{T}}\mathrm{Q} = 1$ with $\det \mathrm{Q} = 1$. Matrix Q represents a rigid-body rotation.

3.1 Two-dimensional splay invariants

For transversely isotropic 2D membranes, the unit vector $\mathbf{e}_f$ in the intrinsic coordinate frame that locates a specific fiber tangent within a given fiber distribution is described via polar coordinates

$$\mathbf{e}_f(\theta) = \cos(\theta)\mathbf{e}_\alpha + \sin(\theta)\mathbf{e}_\beta, \tag{12}$$

where angle θ orients $\mathbf{e}_f$ with respect to the mean-fiber direction $\mathbf{e}_\alpha$ (i.e., to $\mathbf{a}_0$) in the plane of a membrane (viz., the $\alpha\beta$ plane).

We adopt the Gaussian formulation primarily because it allows analytic solutions (cf. Appendix 1, 2). The cosine of the angle between the mean-fiber direction $\mathbf{e}_\alpha$ and that of an individual fiber $\mathbf{e}_f$ is given by the inner product $\mathbf{e}_\alpha \cdot \mathbf{e}_f$, which from Eq. 12 is just cosθ. The Gaussian distribution governing a single fiber family (i.e., transverse isotropy), when expressed in the local coordinate system (α, β, γ) with base vectors $\{\mathbf{e}_\alpha, \mathbf{e}_\beta, \mathbf{e}_\gamma\}$, is therefore simply

$$\frac{1}{\sigma\sqrt{2\pi}} \exp\left(\frac{-\theta^2}{2\sigma^2}\right),$$

with σ being a standard deviation in the angle of fiber dispersion about the mean-fiber direction $\mathbf{e}_\alpha$. Because the local coordinate direction $\mathbf{e}_\alpha$ is coincident with the mean-fiber direction $\mathbf{a}_0$, there is no angle between $\mathbf{e}_\alpha$ and $\mathbf{a}_0$, and as such, the mean angle for this distribution, which is usually denoted by μ, is identically zero—a direct consequence of selecting the intrinsic coordinate system that we did.

In the spirit of Lanir (1983), we propose the following definition for our fourth invariant for 2D splay:

$$I_{\langle\mathrm{IV}\rangle} = \int_{-\pi/2}^{\pi/2} \frac{\exp(-\theta^2/2\varsigma^2)}{\varsigma\sqrt{2\pi}\,\mathrm{erf}(\pi/2\sqrt{2}\varsigma)} \mathbf{e}_f(\theta) \cdot \mathrm{Q}^{\mathrm{T}}\mathrm{CQ}\mathbf{e}_f(\theta)\mathrm{d}\theta, \tag{13}$$

where ς is akin to σ, except that ς is not a standard deviation whose units are radians; ς is a phenomenological parameter. A like expression with C^2 replacing C defines $I_{\langle\mathrm{V}\rangle}$. The error function erf(x) is introduced into these formulae for reasons that are made clear later in Sect. 3.3. These invariants satisfy the required limits: $\lim_{\varsigma\to 0} I_{\langle\mathrm{IV}\rangle}(\varsigma) = I_{\mathrm{IV}}$ and $\lim_{\varsigma\to 0} I_{\langle\mathrm{V}\rangle}(\varsigma) = I_{\mathrm{V}}$; no constraint is imposed a priori on their limits as $\varsigma \to \infty$. In Eq. 13, the right-deformation tensor C is rotated into the local coordinate frame (α, β, γ) by the mapping Q^T CQ, or equivalently, the fiber tangent vector $\mathbf{e}_f$ is rotated into the global coordinate frame (1,2,3) by the mapping $\mathrm{Q}\mathbf{e}_f$, in accordance with Eq. 11.

3.2 Three-dimensional splay invariants

For transversely isotropic 3D tissues, $\mathbf{e}_f$ is located via spherical coordinates

$$\mathbf{e}_f(\theta, \phi) = \cos(\theta)\mathbf{e}_\alpha + \sin(\theta)(\cos(\phi)\mathbf{e}_\beta + \sin(\phi)\mathbf{e}_\gamma), \tag{14}$$

based on the geometry presented in Fig. 1. Here, angles θ and ϕ orient $\mathbf{e}_f$ with respect to the mean-fiber direction $\mathbf{e}_\alpha$ of the embedded frame.

For 3D splay with transverse isotropy, our fourth invariant is defined by

$$I_{\langle\mathrm{IV}\rangle} = \int_0^{2\pi} \int_{-\pi/2}^{\pi/2} \frac{\exp(-\theta^2/2\varsigma^2)}{\varsigma(2\pi)^{3/2}\mathrm{erf}(\pi/2\sqrt{2}\varsigma)} \mathbf{e}_f(\theta, \phi) \cdot \mathrm{Q}^{\mathrm{T}}\mathrm{CQ}\mathbf{e}_f(\theta, \phi)\mathrm{d}\theta\mathrm{d}\phi. \tag{15}$$

A like formula with C^2 replacing C defines $I_{\langle V\rangle}$. The Gaussian distribution is independent of ϕ in these invariants, because of an assumption of isotropy in the transverse plane. Once again, $\lim_{\varsigma\to 0} I_{\langle IV\rangle}(\varsigma) = I_{IV}$ and $\lim_{\varsigma\to 0} I_{\langle V\rangle}(\varsigma) = I_V$.

The fact that a right circular cone is used to describe the angular dispersion of individual fibers implies a radial symmetry in the transverse plane, which is consistent with the notion of transverse isotropy. An elliptic cone could be employed if radial symmetry were deemed inappropriate. We will discuss this case later on, but we do not derive it.

3.3 Intrinsic anisotropic stiffness

We postulate the existence of a material-constant tensor field that we denote as $\kappa(\mathrm{Q}^{\mathrm{T}}\mathbf{X}) = \kappa_{\mu\nu}(\mathrm{Q}^{\mathrm{T}}\mathbf{X})\mathbf{e}_\mu \otimes \mathbf{e}_\nu$, where $\mathbf{e}_\mu = \mathrm{Q}^{\mathrm{T}}\mathbf{e}_i$ and $\mathbf{e}_\nu = \mathrm{Q}^{\mathrm{T}}\mathbf{e}_j$, which serves as a relative (i.e., normalized) stiffness tensor associated with the anisotropic facets of material geometry. For 2D splay, this field is given by

$$\kappa(\varsigma) = \int_{-\pi/2}^{\pi/2} \frac{\exp(-\theta^2/2\varsigma^2)}{\varsigma\sqrt{2\pi}\mathrm{erf}(\pi/2\sqrt{2}\varsigma)} \mathbf{e}_f \otimes \mathbf{e}_f(\theta)\mathrm{d}\theta, \tag{16}$$

and for 3D splay with transverse isotropy, it is given by

$$\kappa(\varsigma) = \int_{0}^{2\pi}\int_{-\pi/2}^{\pi/2} \frac{\exp(-\theta^2/2\varsigma^2)}{\varsigma(2\pi)^{3/2}\mathrm{erf}(\pi/2\sqrt{2}\varsigma)} \mathbf{e}_f \otimes \mathbf{e}_f(\theta,\phi)\mathrm{d}\theta\mathrm{d}\phi, \tag{17}$$

where the global anisotropic material stiffness $\boldsymbol{K}$ introduced in Eq. (18) relates to its intrinsic counterpart κ via

$$\mathrm{K} = \mathrm{Q}\kappa\mathrm{Q}^{\mathrm{T}}. \tag{18}$$

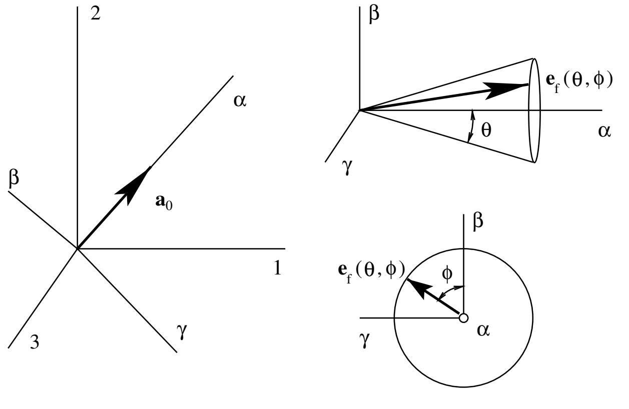

Fig. 1 The diagram on the left relates the global coordinates (1,2,3) to the local coordinates (α , β , γ), selected so that the mean-fiber direction $\mathbf{a}_0$ in the Lagrangian frame aligns with the α-axis. The *diagrams on the right* illustrate how the unit vector $\mathbf{e}_f$ for a specific fiber within a fiber distribution of a 3D tissue is oriented with respect to the mean-fiber direction $\mathbf{a}_0$ via angles θ and ϕ

Both of these $\boldsymbol{\kappa}$ tensors obey the required property: $\lim_{\varsigma\to 0} \mathrm{Q}\boldsymbol{\kappa}(\varsigma)\mathrm{Q}^{\mathrm{T}} = \mathbf{a}_0 \otimes \mathbf{a}_0$, and both of the $\boldsymbol{\kappa}$ tensors are symmetric; therefore, their affiliated $\boldsymbol{K}$ tensors are symmetric too. Analytic solutions to Eqs. 16, 17, and 18 are provided in Appendices 1, 2, respectively. The ability to analytically solve for the anisotropic stiffness K means that this theory will be efficient when implemented into finite-element codes. In contrast, the models of Hurschler et al. (1997), Sacks (2000), and Einstein (2002) all require a numeric integration of splay, which is more costly to implement.

The coefficient $1/\mathrm{erf}(\pi/2\sqrt{2}\varsigma)$ is introduced into Eqs. 16 and 17 to force the trace of $\boldsymbol{\kappa}$ (and therefore of K) to equal the trace of $\mathbf{a}_0 \otimes \mathbf{a}_0$ (viz., $\mathrm{tr}(\mathbf{a}_0 \otimes \mathbf{a}_0) = 1$), which is the only non-zero invariant of tensor $\mathbf{a}_0 \otimes \mathbf{a}_0$. Alternatively, this coefficient can be viewed as that scaling factor which is required to change the limits of integration from $\int_{-\infty}^{\infty}$ to $\int_{-\pi/2}^{\pi/2}$ in the Gaussian distributions present in these formulae. Viewed this way, it is the presence of possibly non-zero second and/or third invariants for K that distinguishes K from $\mathbf{a}_0 \otimes \mathbf{a}_0$.

3.3.1 An approximation

The non-zero components of the analytic solutions to the intrinsic stiffness tensors listed in the appendices are expressed in terms of error functions with complex arguments (e.g., erf(*z*), $z \in \mathbb{C}$). Because this function is not found in most, standard, computer, math libraries, we introduce a simple approximation to the analytic results derived in these appendices that one can readily employ; it being,

$$[[\boldsymbol{\kappa}(\varsigma)]]_{\mu\nu} \approx \begin{bmatrix} \frac{1}{2}(l + \mathrm{e}^{-2\varsigma^2}) & 0 & 0 \\ 0 & \frac{f}{2}(l - \mathrm{e}^{-2\varsigma^2}) & 0 \\ 0 & 0 & \frac{1-f}{2}(l - \mathrm{e}^{-2\varsigma^2}) \end{bmatrix}, \quad 0 \le f \le 1, \tag{19}$$

which is in keeping with the constraint that $\mathrm{tr}\,\boldsymbol{\kappa} = 1$. Parameters $f = 0$ and $f = 1$ apply to 2D splay with the normal to the membrane being in the β- and γ-directions, respectively, while $f = \frac{1}{2}$ applies for 3D splay with transverse isotropy. Splay will be orthotropic whenever $f \neq \frac{1}{2}$; specifically, we conjecture, but do not prove, that there will be an elliptic symmetry in the transverse plane.

The analytic (Appendix 1) and approximate (Eq. 19) solutions for κ are contrasted in Fig. 2 for 2D splay, while the formulae in Appendix 2 and Eq. 19 are contrasted in Fig. 3 for 3D splay with transverse isotropy. As a result, one can easily justify using the approximate solution stated in Eq. 19 over its analytic counterparts derived in the appendices, especially since selecting a Gaussian distribution to describe fiber dispersion was an assumption in the first place.

Substituting Eq. 19 into Eq. 18 quantifies the anisotropic stiffness matrix K that appears in the elastic model of Eqs. 9 and 10 and its associated invariants in Eq. 6.

4 Elasticity for finite elements

Soft tissues are generally considered to be incompressible or nearly incompressible. In a finite-element analysis that involves incompressibility, a standard displacement based interpolation method leads to ill-conditioning of the numerics (Malkus and Hughes 1978). Anticipating like difficulties, following Flory (1961), we seek to decouple pressure from displacement. This decoupling is compatible with two-field displacement-pressure interpolations that avoid volumetric locking in particular, and numerical ill-conditioning in general.

Adopting the approach and notation of Simo and Hughes (1998, pp 358–364) we define

$$J = \det \mathrm{F} = \frac{\varrho_0}{\varrho}, \quad \bar{\mathrm{F}} = J^{-1/3}\mathrm{F}, \quad \bar{\mathrm{C}} = \bar{\mathrm{F}}^{\mathrm{T}}\bar{\mathrm{F}}, \quad \bar{\mathrm{B}} = \bar{\mathrm{F}}\bar{F}^{T}, \tag{20}$$

so that $\det \bar{\mathrm{F}} = 1$, and therefore, $\det \bar{\mathrm{B}} = \det \bar{\mathrm{C}} = 1$. The strain-energy density W is hypothesized to decouple as (Holzapfel and Weizsäcker 1998)

$$\varrho_0 W(\mathrm{C}) = \widetilde{\mathcal{W}}(J) + \overline{\mathcal{W}}(\bar{\mathrm{C}}) + \widehat{\mathcal{W}}(\mathrm{K}, \bar{\mathrm{C}}), \tag{21}$$

where $\widetilde{\mathcal{W}}, \overline{\mathcal{W}}$ and $\widehat{\mathcal{W}}$ are the dilational, distortional-isotropic and distortional-anisotropic strain energies, respectively.

The above definitions allow the general constitutive equation for elasticity stated in Eq. 8 to be recast as (Simo and Hughes 1998, p 360)

$$\mathrm{S} = J\frac{\partial\widetilde{\mathcal{W}}(\Theta)}{\partial\Theta}\mathrm{C}^{-1} + 2J^{-2/3}\left(\mathrm{DEV}\left[\frac{\partial\overline{\mathcal{W}}(\bar{\mathrm{C}})}{\partial\bar{\mathrm{C}}}\right] + \mathrm{DEV}\left[\frac{\partial\widehat{\mathcal{W}}(\mathrm{K},\bar{\mathrm{C}})}{\partial\bar{\mathrm{C}}}\right]\right), \tag{22}$$

so that, when pushed forward into the Eulerian frame, it becomes

$$\tau = J\frac{\partial\widetilde{\mathcal{W}}(\Theta)}{\partial\Theta}\mathbf{I} + \mathbf{2}\left(\mathrm{dev}\left[\bar{\mathrm{F}}\frac{\partial\overline{\mathcal{W}}(\bar{\mathrm{C}})}{\partial\bar{\mathrm{C}}}\bar{\mathrm{F}}^{\mathrm{T}}\right] + \mathrm{dev}\left[\bar{\mathrm{F}}\frac{\partial\widehat{\mathcal{W}}(\mathrm{K},\bar{\mathrm{C}})}{\partial\bar{\mathrm{C}}}\bar{\mathrm{F}}^{\mathrm{T}}\right]\right), \tag{23}$$

wherein

$$\begin{aligned} \mathrm{DEV}[\bullet] &= (\bullet) - \frac{1}{3}\mathrm{tr}((\bullet)\mathrm{C})\mathrm{C}^{-1} \quad \text{and} \\ \mathrm{dev}[\bullet] &= (\bullet) - \frac{1}{3}\mathrm{tr}(\bullet)\mathbf{I} \end{aligned} \tag{24}$$

are the respective Lagrangian and Eulerian deviatoric operators. Tensors $\bar{\mathrm{F}}$ and $J\mathrm{I}$ are the deviatoric (volume preserving) and dilational (volume changing) parts of the deformation gradient F, respectively. Although $\Theta \equiv J$ in a mathematical sense, we follow the admonition of Simo and Hughes and maintain their distinction, to remind ourselves that displacement and pressure are to be interpolated separately in finite-element codes suitable for soft-tissue analysis.

4.1 A simple model

The spherical strain-energy model advocated by Simo and Taylor (1991) is

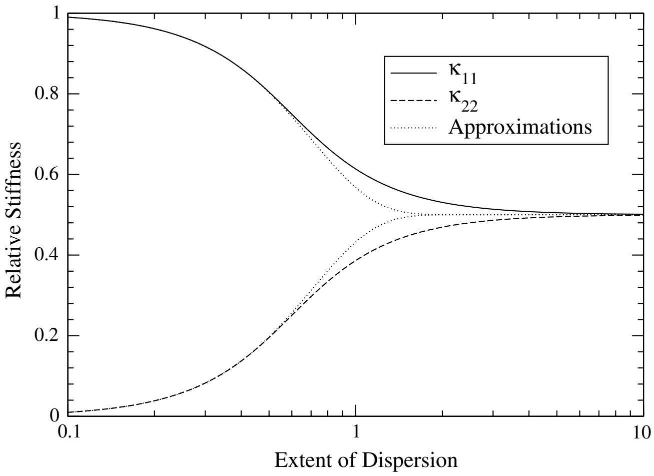

Fig. 2 Plots of relative stiffness versus fiber dispersion parameter ς for 2D splay, as determined by Eq. 19 with $f=1$ for the approximate solutions, and by Eqs. 49 and 50 for the analytic solutions

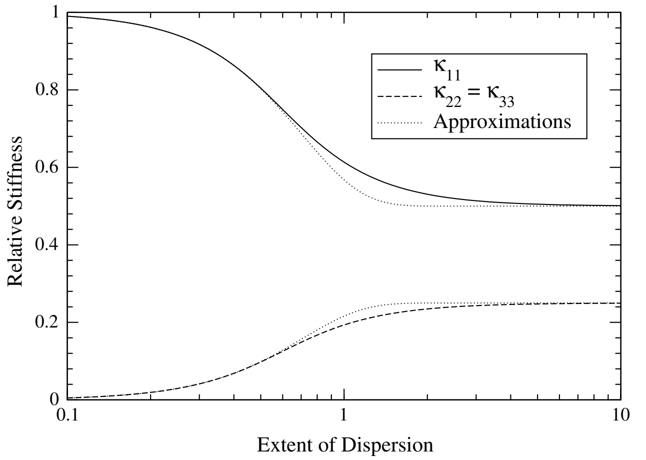

Fig. 3 Plots of relative stiffness versus fiber dispersion parameter ς for transversely isotropic 3D splay, as determined by Eq. 19 with $f=1/2$ for the approximate solutions, and by Eqs. 54 and 55 for the analytic solutions

$$\widehat{\mathcal{W}}(\Theta) = \kappa \frac{1}{2}\left(\frac{1}{2}(\Theta^2 - 1) - \ln \Theta\right), \tag{25}$$

where κ is the bulk modulus. Many functional forms have been advanced over the years for quantifying dilatation. Equation 25 is recommended because it is a convex function[3] (Hartmann and Neff 2003), and because its gradient leads to a second-order accurate approximation of the Hencky (1928) definition for dilatation [4] (Freed 2004). Equation 25 is appropriate for the mean-dilation integration schemes used in some finite-element codes.

Equation 25 does not, however, fit the constraint criteria of the u/p finite-element scheme advocated by Sussman and Bathe (1987). Thus, if this interpolation scheme is adopted, then

$$\widehat{\mathcal{W}}(\Theta) = \kappa \frac{1}{2}(J - 1)^2, \tag{26}$$

is mandated as the dilational strain-energy model. In these codes there is no distinction made between J and Θ.

Seeking an isotropic contribution to the deviatoric strain energy with attributes akin to those affiliated with the dilational part (viz., a convex function whose gradient produces a second-order accurate approximation of true strain), we assign

$$2\overline{\mathcal{W}}(\bar{\mathrm{C}}) = \mu \frac{1}{4}\left(\mathrm{tr}\bar{\mathrm{C}} + \mathrm{tr}\, \bar{\mathrm{C}}^{-1} - 6\right), \tag{27}$$

where μ is the shear modulus, with $\bar{\mathrm{C}}^{-1} = \{\bar{\mathrm{C}}^2 - \mathrm{tr}(\bar{\mathrm{C}})\bar{\mathrm{C}} + \frac{1}{2}\left[(\mathrm{tr}\bar{\mathrm{C}})^2 - \mathrm{tr}\bar{\mathrm{C}}^2\right]\mathrm{I}\}/\det\bar{\mathrm{C}}$ from the Cayley–Hamilton theorem. Tensor $\bar{\mathrm{C}}^{-1}$ exists because $\det\bar{\mathrm{C}} = 1$; consequently, $I_{\mathrm{II}}(\bar{\mathrm{C}}) = \frac{1}{2}\left[(\mathrm{tr}\bar{\mathrm{C}})^2 - \mathrm{tr}\bar{\mathrm{C}}^2\right] = \mathrm{tr}\bar{\mathrm{C}}^{-1} = I_{\mathrm{I}}(\bar{\mathrm{C}}^{-1})$, which appears above. A Mooney (1940) material has different material constants assigned to invariants $\mathrm{tr}\bar{\mathrm{C}}$ and $\mathrm{tr}\bar{\mathrm{C}}^{-1}$, in general, and in this sense, our model is a Mooney material of special form whose constants are equal. Equation 27 has one material parameter, viz., μ; the Mooney material has two parameters; other models have even more. Here, we seek simple relations with respect to the number of unknown material parameters.

For an anisotropic contribution to the deviatoric strain energy, going back to the precept that energy is the area under a force/displacement curve, we advocate that

$$\widehat{\mathcal{W}}(\mathrm{K}, \bar{\mathrm{C}}) = \int_{1}^{[\mathrm{tr}(\mathrm{K}\bar{\mathrm{C}})]^{1/2}} \sigma(\lambda)\mathrm{d}\lambda, \tag{28}$$

where the fiber stress σ is allowed to be an arbitrary function of fiber stretch λ; it is generally nonlinear in biological tissues. The upper limit of integration is the fourth invariant, as it pertains to the deviatoric part of the deformed state. In order for this strain-energy function to be convex, it is necessary that $E_t(\lambda) > \sigma_e(\lambda)$ for all $\lambda > 0$, wherein

$$E_t(\lambda) = \frac{\mathrm{d}\sigma(\lambda)}{\mathrm{d}\lambda} \quad \text{and} \quad \sigma_e(\lambda) = \frac{\sigma(\lambda)}{\lambda}, \tag{29}$$

which are the tangent modulus and engineering stress, respectively, of a fiber whose stretch λ is quantified by

$$\lambda = \left(\mathrm{tr}(\mathrm{K}\bar{\mathrm{C}})\right)^{1/2} = \left(\mathrm{tr}\left(\bar{\mathrm{F}}\mathrm{K}\bar{\mathrm{F}}^{\mathrm{T}}\right)\right)^{1/2}. \tag{30}$$

A physiologically based material model for $\sigma(\lambda)$ has recently been derived by Freed and Doehring (2005) that applies to crimped collagen fibers, which we have extended to meet our needs in Appendix 3

Substituting the strain energies of Eqs. 25, 27, and 28 into Eq. 22 produces an elastic constitutive model suitable for soft-tissue mechanics that when expressed in the Lagrangian frame becomes

$$\begin{aligned}\mathrm{S} = {} & \kappa J \frac{1}{2}(\Theta - \Theta^{-1})\mathrm{C}^{-1} + \mu J^{\frac{-2}{3}}\mathrm{DEV}\left[\frac{1}{4}\left(\mathrm{I} - \bar{\mathrm{C}}^{-2}\right)\right] \\ & + \sigma_e(\lambda) J^{\frac{-2}{3}}\mathrm{DEV}[\mathrm{K}],\end{aligned} \tag{31}$$

or equivalently, when substituted into Eq. 23, becomes

$$\begin{aligned}\tau = {} & \kappa J \frac{1}{2}(\Theta - \Theta^{-1})\mathrm{I} + \mu\, \mathrm{dev}\left[\frac{1}{4}\left(\bar{\mathrm{B}} - \bar{\mathrm{B}}^{-1}\right)\right] \\ & + \sigma_e(\lambda)\mathrm{dev}\left[\bar{\mathrm{F}}\mathrm{K}\bar{\mathrm{F}}^{\mathrm{T}}\right],\end{aligned} \tag{32}$$

when expressed in the Eulerian frame. The strain measure $\frac{1}{2}\left(\Theta - \Theta^{-1}\right)$ is a second-order accurate approximation of Hencky's dilational strain field $\ln\det\mathrm{F}$, while the strain tensor $\frac{1}{4}(\bar{\mathrm{B}} - \bar{\mathrm{B}}^{-1})$ is a second-order accurate approximation of the distortional true-strain field $\ln\bar{\mathrm{V}}$.

4.2 Tangent moduli

The relationship between S and C in Eq. 31 is nonlinear. To obtain a finite-element solution with an iterative Newton-type solution process, that relationship must be linearized with respect to an incremental displacement. This involves the specification of a tangent modulus $\mathbb{C} = \mathbb{C}_{ijk\ell}\mathbf{e}_i \otimes \mathbf{e}_j \otimes \mathbf{e}_k \otimes \mathbf{e}_\ell$—a fourth-rank tensor not to be confused with the second-rank right-deformation tensor $\mathrm{C} = C_{ij}\mathbf{e}_i \otimes \mathbf{e}_j$. To obtain this tangent, stress S is linearized over some interval $[t_n, t_{n+1}]$ such that $\mathrm{S}_{n+1} = \mathrm{S}_n + \mathbb{C}_n\Delta\mathrm{E}$ with $\Delta\mathrm{E} = \mathrm{E}_{n+1} - \mathrm{E}_n = \frac{1}{2}\left(\mathrm{C}_{n+1} - \mathrm{C}_n\right) = \mathrm{F}_n^{\mathrm{T}}\hat{\mathrm{E}}(\mathbf{x}_n; t_n, t_{n+1})\mathrm{F}_n$. Said differently, the tangent modulus corresponds to the slope affiliated with a forward-Euler integration step, and since it depends on step number n, it needs to be re-evaluated at each step along the solution path.

---

[3] $\partial^2\widehat{\mathcal{W}}/\partial\Theta^2 = \frac{1}{2}\kappa(1 + \Theta^{-2}) > 0$, as $\Theta > 0$ due to the conservation of mass

[4] $e = \ln\det\mathrm{F} \approx \frac{1}{2}(\det\mathrm{F} - \det\mathrm{F}^{-1})$

Tensor $\mathbb{C}_n = 2\partial \mathrm{S}/\partial \mathrm{C}_n = 4\varrho_0 \partial^2 W/\partial \mathrm{C}_n \partial \mathrm{C}_n$ defines the tangent modulus in the Lagrangian frame, which can be pushed forward, component by component, into an Eulerian frame according to the mapping $\mathrm{c}^n_{ijk\ell} = F^n_{iI} F^n_{jJ} F^n_{kK} F^n_{\ell L} \mathbb{C}^n_{IJKL}$ at the nth time step that when applied to the next step becomes the tangent modulus of an updated Lagrangian frame. Constructing the components of $\mathbb{C}_n$ in Voigt notation is addressed in Appendix 4.

From Eq. 21, suppressing the subscript n designating step number, the tangent modulus takes on the form

$$\mathbb{C} = \widetilde{\mathbb{C}}(\Theta) + \overline{\mathbb{C}}(\bar{\mathrm{C}}) + \widehat{\mathbb{C}}(\mathrm{K}, \bar{\mathrm{C}}), \tag{33}$$

where, through an application of the chain rule, one obtains

$$\begin{aligned}
\widetilde{\mathbb{C}} &= 4\frac{\partial^2 \widetilde{\mathcal{W}}(\Theta)}{\partial \mathrm{C} \partial \mathrm{C}} \\
&= 4\left(\frac{\partial^2 \widetilde{\mathcal{W}}(\Theta)}{\partial \Theta^2} \frac{\partial \Theta}{\partial \mathrm{C}} \otimes \frac{\partial \Theta}{\partial \mathrm{C}} + \frac{\partial \widetilde{\mathcal{W}}(\Theta)}{\partial \Theta} \frac{\partial^2 \Theta}{\partial \mathrm{C} \partial \mathrm{C}} \right), \\
\overline{\mathbb{C}} &= 4\frac{\partial^2 \overline{\mathcal{W}}(\bar{\mathrm{C}})}{\partial \mathrm{C} \partial \mathrm{C}} \\
&= 4\left(\left(\frac{\partial \bar{\mathrm{C}}}{\partial \mathrm{C}} \right)^{\mathrm{T}} : \frac{\partial^2 \overline{\mathcal{W}}(\bar{\mathrm{C}})}{\partial \bar{\mathrm{C}} \partial \bar{\mathrm{C}}} : \frac{\partial \bar{\mathrm{C}}}{\partial \mathrm{C}} + \frac{\partial \overline{\mathcal{W}}(\bar{\mathrm{C}})}{\partial \bar{\mathrm{C}}} : \frac{\partial^2 \bar{\mathrm{C}}}{\partial \mathrm{C} \partial \mathrm{C}} \right), \\
\widehat{\mathbb{C}}; &= 4\frac{\partial^2 \widehat{\mathcal{W}}(\mathrm{K}, \bar{\mathrm{C}})}{\partial \mathrm{C} \partial \mathrm{C}} \\
&= 4\left(\left(\frac{\partial \bar{\mathrm{C}}}{\partial \mathrm{C}} \right)^{\mathrm{T}} : \frac{\partial^2 \widehat{\mathcal{W}}(\mathrm{K}, \bar{\mathrm{C}})}{\partial \bar{\mathrm{C}} \partial \bar{\mathrm{C}}} : \frac{\partial \bar{\mathrm{C}}}{\partial \mathrm{C}} + \frac{\partial \widehat{\mathcal{W}}(\mathrm{K}, \bar{\mathrm{C}})}{\partial \bar{\mathrm{C}}} : \frac{\partial^2 \bar{\mathrm{C}}}{\partial \mathrm{C} \partial \mathrm{C}} \right),
\end{aligned} \tag{34}$$

with (cf., Holzapfel 2000, p 229)

$$\frac{\partial \bar{C}_{ij}}{\partial C_{k\ell}} = J^{-2/3} \left(I_{ik} I_{j\ell} - \frac{1}{3} C_{ij} C^{-1}_{k\ell} \right), \tag{35}$$

and

$$\begin{aligned}
\frac{\partial^2 \bar{C}_{ij}}{\partial C_{k\ell} \partial C_{mn}} = \frac{1}{3} J^{\frac{-2}{3}} \bigg(C_{ij} \left(C^{-1}_{km} C^{-1}_{\ell n} + \frac{1}{3} C^{-1}_{k\ell} C^{-1}_{mn} \right) \\
- I_{ik} I_{j\ell} C^{-1}_{mn} - C^{-1}_{k\ell} I_{im} I_{jn} \bigg),
\end{aligned} \tag{36}$$

written in component form.

For the preferred volumetric strain energy in Eq. 25, which can be implemented into finite-element codes that use a reduced/selective integration scheme (Malkus and Hughes 1978), one arrives at the following pressure tangent modulus [5]

$$\widetilde{\mathbb{C}} = 2\kappa \left(\left(1 + \Theta^{-2}\right) \frac{\partial \Theta}{\partial \mathrm{C}} \otimes \frac{\partial \Theta}{\partial \mathrm{C}} + \left(\Theta - \Theta^{-1}\right) \frac{\partial^2 \Theta}{\partial \mathrm{C} \partial \mathrm{C}} \right), \tag{37}$$

where the gradients $\partial \Theta/\partial \mathrm{C} \otimes \partial \Theta/\partial \mathrm{C}$ and $\partial^2 \Theta/\partial \mathrm{C} \partial \mathrm{C}$ are handled by the element technology of the particular finite element being employed. Alternatively, in an u/p formulation (Sussman and Bathe 1987), the pressure tangent modulus corresponding to Eq. 26 is given by[6]

$$\begin{aligned}
\widetilde{\mathbb{C}} = \kappa J \Big(J \mathrm{C}^{-1} \otimes \mathrm{C}^{-1} \\
+ (1 - J) \left(2\mathrm{C}^{-1} \odot \mathrm{C}^{-1} - \mathrm{C}^{-1} \otimes \mathrm{C}^{-1} \right) \Big),
\end{aligned} \tag{38}$$

where now the gradients $\partial \Theta/\partial \mathrm{C} \otimes \partial \Theta/\partial \mathrm{C}$ and $\partial^2 \Theta/\partial \mathrm{C} \partial \mathrm{C}$ are handled by us, the constitutive developers, as there is no distinction made between Θ and J in these codes.

The isotropic tangent modulus corresponding to Eq. 27 is determined to be

$$\begin{aligned}
\overline{\mathbb{C}} = \mu \Big\{ J^{\frac{-2}{3}} \Big[\mathrm{C}^{-1} \boxtimes \mathrm{C}^{-2} - \frac{1}{3} \left(\mathrm{C}^{-1} \otimes \mathrm{C}^{-2} + \mathrm{C}^{-2} \otimes \mathrm{C}^{-1} \right) \\
+ \frac{1}{9} \left(\mathrm{tr} \mathrm{C}^{-1} \right) \mathrm{C}^{-1} \otimes \mathrm{C}^{-1} \Big] + \frac{1}{6} \Big[\left(J^{\frac{-2}{3}} \mathrm{tr} \mathrm{C} - J^{\frac{2}{3}} \mathrm{tr} \mathrm{C}^{-1} \right) \\
\times \left(\mathrm{C}^{-1} \odot \mathrm{C}^{-1} + \frac{1}{3} \mathrm{C}^{-1} \otimes \mathrm{C}^{-1} \right) \\
- \mathrm{C}^{-1} \otimes \left(J^{\frac{-2}{3}} \mathrm{I} - J^{\frac{2}{3}} \mathrm{C}^{-2} \right) - \left(J^{\frac{-2}{3}} \mathrm{I} - J^{\frac{2}{3}} \mathrm{C}^{-2} \right) \otimes \mathrm{C}^{-1} \Big] \Big\}.
\end{aligned} \tag{39}$$

All three tensor dyadic operators are present in this result, viz., $\otimes$, $\odot$ and $\boxtimes$.

Lastly, the anisotropic tangent modulus corresponding to ‘Eq. 28 is given by

$$\begin{aligned}
\widehat{\mathbb{C}} = J^{-2/3} \Big\{ \left(E_t(\lambda) - \sigma_e(\lambda) \right) \Big(J^{\frac{-2}{3}} \lambda^{-2} \mathrm{K} \otimes \mathrm{K} \\
- \frac{1}{3} \left(\mathrm{K} \otimes \mathrm{C}^{-1} + \mathrm{C}^{-1} \otimes \mathrm{K} \right) + \frac{1}{9} J^{\frac{2}{3}} \lambda^2 \mathrm{C}^{-1} \otimes \mathrm{C}^{-1} \Big) \\
+ \frac{2}{3} \sigma_e(\lambda) \Big(J^{\frac{2}{3}} \lambda^2 \left(\mathrm{C}^{-1} \odot \mathrm{C}^{-1} + \frac{1}{3} \mathrm{C}^{-1} \otimes \mathrm{C}^{-1} \right) \\
- \mathrm{K} \otimes \mathrm{C}^{-1} - \mathrm{C}^{-1} \otimes \mathrm{K} \Big) \Big\},
\end{aligned} \tag{40}$$

which utilizes tensor dyadic operators $\otimes$ and $\odot$, but not $\boxtimes$.

5 Collagen models

The fiber tangent modulus $E_t(\lambda)$ and engineering stress $\sigma_e(\lambda)$ present in Eq. 40 are defined in Eq. 29, whose stretch λ is established in Eq. 30. It is worth noting that the terms in the fourth-rank tensor representing the anisotropic tangent modulus are completely independent of the specific collagen fiber model chosen. This implies that a modification of fiber stress–strain law requires no reformulation of the constitutive tangent matrix, making the model very flexible for different types of soft tissues. This is not the case with constitutive models represented by Eq. 1.

---

[5] These tensor gradients are useful when deriving the subsequent tangent moduli:
$\frac{\partial \mathrm{Z}}{\partial \mathrm{Z}} = \mathrm{I} \odot \mathrm{I}, \quad \frac{\partial \mathrm{Z}^{-1}}{\partial \mathrm{Z}} = -\mathrm{Z}^{-1} \odot \mathrm{Z}^{-1}, \quad \mathrm{Z} = \mathrm{Z}^{\mathrm{T}}, \quad \det \mathrm{Z} \neq 0,$
where $(\mathrm{Z}^{-1} \odot \mathrm{Z}^{-1})_{ijk\ell} = \frac{1}{2} \left(Z^{-1}_{ik} Z^{-1}_{j\ell} + Z^{-1}_{i\ell} Z^{-1}_{jk} \right)$ in the notation of Holzapfel (2000, p. 254).

[6] The outer-dyadic tensor product $(\mathrm{A} \otimes \mathrm{B})_{ijk\ell} = A_{ij} B_{k\ell}$, and the inner-dyadic tensor product $(\mathrm{A} \boxtimes \mathrm{B})_{ijk\ell} = \frac{1}{4}(A_{ik} B_{j\ell} + A_{i\ell} B_{jk} + A_{jk} B_{i\ell} + A_{j\ell} B_{ik})$, are established in Appendix 4. Whenever A and B are the same tensor field—say, A—then the inner-dyadic product $\mathrm{A} \boxtimes \mathrm{A}$ simplifies to $\mathrm{A} \odot \mathrm{A}$, i.e., $\mathrm{A} \boxtimes \mathrm{A} = \mathrm{A} \odot \mathrm{A}$.

In the Examples section that follows, two collagen stress-strain models are used. The first is the rule adopted by Billiar and Sacks (2000b) for aortic valve tissue; it being,

$$\sigma(\lambda) = A\left(\mathrm{e}^{B(\lambda^2-1)/2} - 1\right), \tag{41}$$

thus the two required terms in Eq. 40 are

$$\begin{aligned} \sigma_e(\lambda) &= A\lambda^{-1}\left(\mathrm{e}^{B(\lambda^2-1)/2} - 1\right) \quad \text{and} \\ E_t(\lambda) &= AB\lambda\mathrm{e}^{B(\lambda^2-1)/2}. \end{aligned} \tag{42}$$

As an alternative to this phenomenological model, we also employ the structural model of Freed and Doehring (2005) that is based on the physiology of crimped collagen fibers. An adaptation of their algorithm is given in Appendix 3 (see Algorithm 1). Specifically, given a fiber stretch λ, this model returns the stress σ/λ and tangent modulus $\mathrm{d}\sigma/\mathrm{d}\lambda$ of the fiber. There are four physiological parameters (material constants defined at the top of the algorithm) that the user must supply.

To implement either of these two models in finite elements, or any other model for that matter, it is sufficient to change the lines of code corresponding to the scalar values $E_t(\lambda)$ and $\sigma_e(\lambda)$. This opens up the possibility of coding the material model once and selecting an appropriate fiber model with a passed parameter.

6 Examples

We offer our invariant theory as a computationally efficient alternative to statistical structural models of the type represented by Eq. 1.

In the examples that follow, we match Eq. 31 to biaxial data for fresh aortic valve tissue. These data were generously supplied by Dr. Sacks from the Engineered Tissue Mechanics Laboratory at the University of Pittsburgh, and have been reported on elsewhere (Billiar and Sacks 2000a). In the first example, we adopt an exponential fiber stress–strain rule—the same phenomenological model used by (Billiar and Sacks 2000b). In the second example, we adopt a structurally based collagen fiber model recently derived by Freed and Doehring (2005).

The original data were provided in the format of Lagrangian membrane tension; that is, force per unit reference length. To characterize the constitutive model, it was necessary to convert the data to Lagrangian stress. Thus, a thickness of 0.6 mm was assumed. It must also be noted that these data do not comprise a complete biaxial set, in the sense that there were finite off-axis deformation terms (i.e., $F_{12} \neq F_{21} \neq 0$, cf. Fig. 4) with no concomitant measurement of an off-axis stress. As such, it was necessary to convert Eq. 31 into its first Piola-Kirchhoff stress (i.e. $\mathrm{P} = \mathrm{FS}$) counterpart for parameter estimation.

An adaptive grid refinement (AGR) global optimization algorithm was implemented in Mathematica (Wolfram Research Incorporated, Champagne, IL, USA), using a commercially available global optimization algorithm (Global Optimization, Loehle Enterprises, Naperville, IL, USA) (Doehring et al. 2004). Parameters were simultaneously fit to five separate biaxial load protocols, corresponding to fiber-to-cross-fiber membrane stress ratios of 30:60, 45:60, 60:60, 60:45, and 60:30 N/m. These were the same protocols used to fit the data in the original publications by Billiar and Sacks (2000a, b). During the estimation process, the membranes were considered to be incompressible, and the shear modulus pertaining to the isotropic response was set to zero. The objective function for the global minimum was defined as

$$\begin{aligned} \text{error} = \sum_{j=1}^{5} \left(\frac{\sum_{i=1}^{N_j} \left(P_{11}^{\text{model}} - P_{11}^{\text{data}}\right)_{ij}^2}{\sum_{i=1}^{N_j} \left(P_{11}^{\text{data}}\right)_{ij}^2} \right. \\ \left. + \frac{\sum_{i=1}^{N_j} \left(P_{22}^{\text{model}} - P_{22}^{\text{data}}\right)_{ij}^2}{\sum_{i=1}^{N_j} \left(P_{22}^{\text{data}}\right)_{ij}^2} \right), \end{aligned} \tag{43}$$

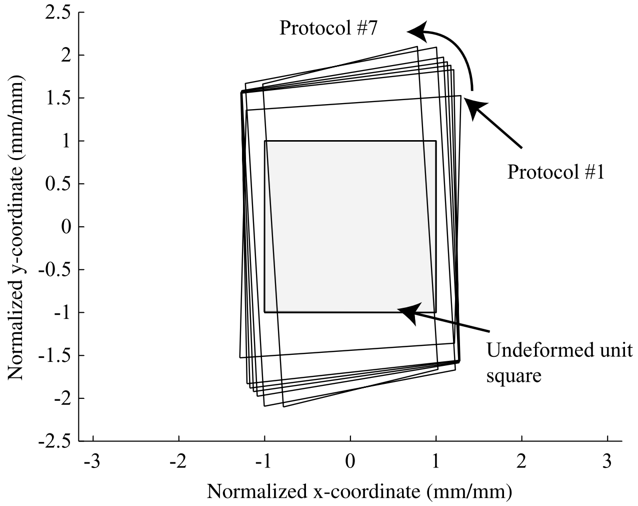

Fig. 4 Mapping of a unit square to the current configuration, corresponding to the last data point of each of the seven protocols of Billiar and Sacks (2000a). Note that there exist finite $F_{12} \neq F_{21}$ terms

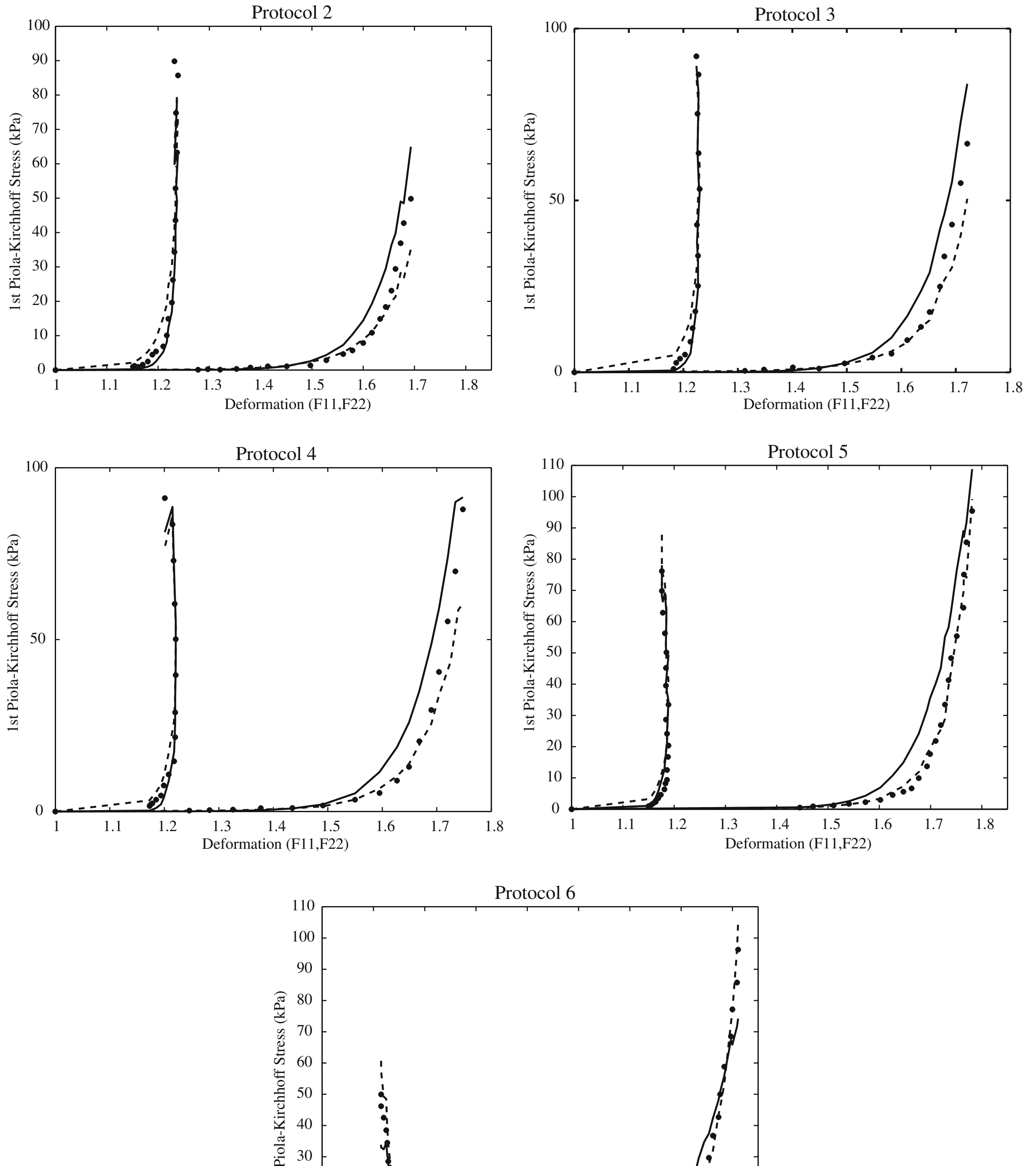

Fig. 5 Constitutive model fit to biaxial data from fresh aortic valve tissue: exponential fiber stress–strain rule (*left*: fiber direction, *right*: cross-fiber direction). *Dots* are the original data. *Solid lines* are from our constitutive model Eqs. 31 and 42. *Dashed lines* are from the statistical model in Eq. 44 with Eq. 45 for the stress/stretch law

where P_{11} corresponds to the fiber direction, P_{22} corresponds to the cross-fiber direction, and N_j represents the number of data points for the jth protocol.

6.1 Exponential fiber model

In this example, we specifically compare our constitutive model to both the data and to a statistical structural model with an exponential fiber stress that was proposed in Billiar and Sacks (2000b) and implemented by Einstein (2002) whose fiber stress is

$$\mathrm{S}^f = J^{\frac{-2}{3}}\mathrm{DEV}\left[\int_{-\pi/2}^{\pi/2} S_f(\theta,\bar{\mathrm{C}})R(\theta)\mathbf{a}_0\otimes\mathbf{a}_0(\theta)\mathrm{d}\theta\right], \tag{44}$$

where the fiber stress–strain law $S_f(\theta,\bar{\mathrm{C}})$ and the probability density function $R(\theta)$ are given by

$$S_f(\theta,\bar{\mathrm{C}}) = A\left(\mathrm{e}^{B\left(\mathbf{a}_0(\theta)\cdot\bar{\mathrm{C}}\mathbf{a}_0(\theta)-1\right)/2}-1\right) \quad \text{and}$$

$$R(\theta) = \frac{\exp\left(-\theta^2/2\sigma^2\right)}{\sigma\sqrt{2\pi}}. \tag{45}$$

The fiber stress $\sigma_e(\lambda)$ for Eq. 31 is given by Eq. 42.

Optimized parameters for the constitutive model based on our new invariant theory (Eqs. 31, 42) were: $A = 0.007$, $B = 21.6$, and $\varsigma = 0.795$ when fit against the data presented in Fig. 5. Parameters for the constitutive model based on the statistical structure of Eqs. 44 and 45 were: $A = 0.045$, $B = 21.0$, and $\sigma = 0.192$. Although the units for σ in Eq. 45 are radians, our ς parameter in Eq. 19 is not strictly an angle. To force the consistency constraint $\lim_{\varsigma\to 0}\mathrm{Q}\boldsymbol{\kappa}(\varsigma)\mathrm{Q}^{\mathrm{T}} = \mathbf{a}_0\otimes\mathbf{a}_0$ required us to introduce a scaling factor of $1/\mathrm{erf}\left(\pi/2\sqrt{2}\varsigma\right)$ into $R(\theta)$.

Overall, the fit was quite good for both models (see Fig. 5). The error calculated via Eq. 43 for the invariant model of Eqs. 31 and 42 was 0.40, as opposed to an error of 0.45 for the model of Eqs. 44 and 45. On average, Eqs. 31 and 42 tended to fit the fiber-direction stress slightly better, while Eqs. 44 and 45 tended to fit the cross-fiber stress slightly better. With regard to our constitutive model only, the toe-region of the stress–strain curve (commonly viewed as a transition between the extinction of collagen crimp and the linear behavior of straightened collagen) was slightly under-predicted in the fiber direction and over-predicted in the cross-fiber direction.

6.2 Crimped collagen model

Because the modulus $E_t(\lambda)$ and stress $\sigma_e(\lambda)$ are generic scalar components of the anisotropic tangent modulus in Eq. 40, we are free to adopt any reasonable fiber stress–strain rule, without making the complexity due to tangent modulus construction prohibitive. This is a desirable precondition for finite-element analysis.

As our second example, consider the micro-structurally based collagen fiber stress–strain rule based on the physiology of crimped collagen fibers that was recently proposed by Freed and Doehring (2005) (Algorithm 1 in Appendix 3). This is an algorithm for the elastic response of crimped collagen fibers, based on the observation that fibril crimp has a three-dimensional structure at the micrometer scale whose geometry can be approximated as a cylindrical helix. For pre-failure analysis, the model is defined in terms of three physiological parameters: the initial normalized wavelength of the crimp H_0/r_0, the initial normalized amplitude of the crimp R_0/r_0, and the elastic modulus of the collagen fiber in the linear region E_f. Parameters H_0 and R_0 are normalized with respect to fibril radius r_0.

Values for these parameters were estimated at: $H_0/r_0 = 14.4$, $R_0/r_0 = 2.19$, $E_f =$ 10.6 MPa, and $\varsigma = 0.768$. Overall, the fit of this variation of our constitutive model was excellent (see Fig. 6), with an error of 0.37. Only the predictions for the sixth protocol have a significant difference from the data.

7 Finite-element implementations

Equation 31 and Algorithm 1 from Appendix 3 were implemented into Adina (Adina R&D Inc., Watertown, MA, USA) where a two-field pressure/displacement interpolation is employed (Sussman and Bathe 1987). Using this compute engine, numeric experiments were performed to demonstrate the effect that splay has on the predicted state of stress. The results are shown in Fig. 7. Values for the material constants used to construct this figure were the same as those used in Fig. 6, except for the splay variable ς (see Fig. 2) which is varied in Fig. 7. Equibiaxial extensions were imposed for deformations up to $F_{11} = F_{22} = 1.4$.

Additionally, Eq. 31 and Algorithm 1 from Appendix 3 were both implemented into LS-DYNA (Livermore Software Technology Corporation, Livermore, CA, USA), where a mean-dilation pressure/displacement interpolation was imposed. Using this compute engine, we simulated a dynamic in vacuo bioprosthestic aortic valve model. A total of 5,400 C^1 brick elements were used. Principle fiber angles were circumferential. Fixed displacement and rotation boundary conditions were applied to three sides of each leaflet. Pressure, applied on the ventricular face, was ramped from 0 kPa to 0.5 kPa (3.5 mmHg) then decreased linearly to -10 kPa (80 mmHg). Pinball segment-based contact, with warped segment checking and a search depth of 3, was defined between the three leaflets. The identical simulation, adopting the same fiber model (Algorithm 1 from Appendix 3), was run with a constitutive model based on the statistical structure of Eq. 45 and the Gaussian from Eq. 44. Material constants were the same except for the

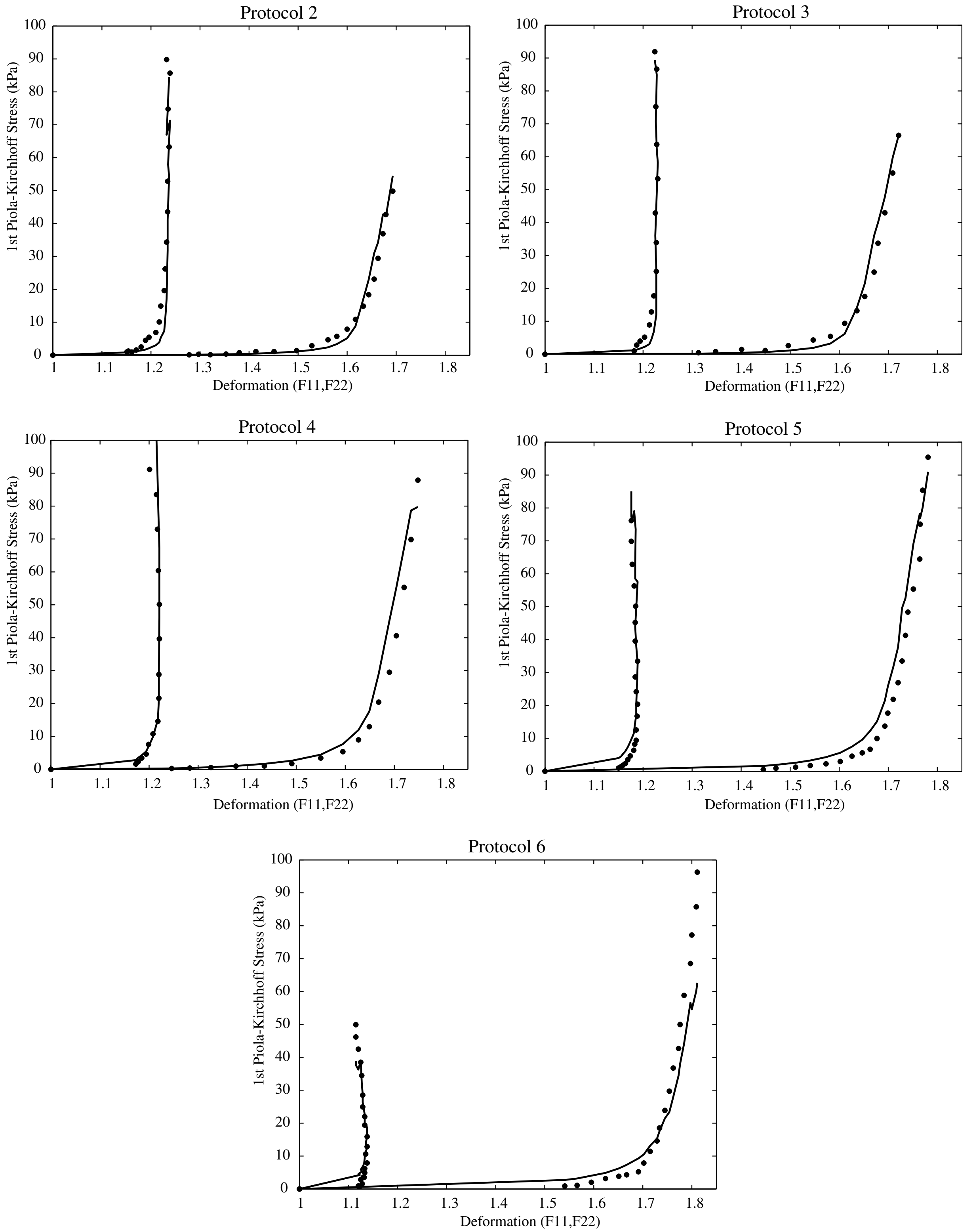

Fig. 6 Constitutive model fit to biaxial data from fresh aortic-valve tissue: fiber crimp stress–strain rule (*left*: fiber direction, *right*: cross-fiber direction). *Dots* are the original data. *Solid lines* are our constitutive model Eq. 31 using Algorithm 1 from Appendix 3 for the stress/stretch law

splay variable, which was set to 0.192, consistent with previous estimations. LS-DYNA is primarily an explicit code, thus the time step is governed by the speed of sound in the tissue, which in the context of nonlinear continuum mechanics is a function of the current deformation field. To facilitate a comparison of the computational efficiency of the two formulations, the sound speed was set to $c^2 = (\kappa + E_f)/\rho$ for both simulations. Therefore, differences in CPU time between the two material-model simulations were the result of computational efficiency alone.

Figure 8 shows the fully opened and fully closed configurations of solutions based on Eq. 31 and Algorithm 1 from Appendix 3 (see 8A, B), and on Eqs. 44 and 45 with the fiber model from Algorithm 1 from Appendix 3 (see 8C, D). The deformed configurations and maximum principle stresses between the two models are comparable. CPU times were 6,424 s for the invariant formulation and 16,968 s for the integrated statistical model. Both simulations were run on a Linux machine with a 2.4 GHz Pentium IV processor and 2 GB of memory. Thus, our invariant formulation for fiber dispersion ran 2.64 times faster than the simulation based on integrated splay.

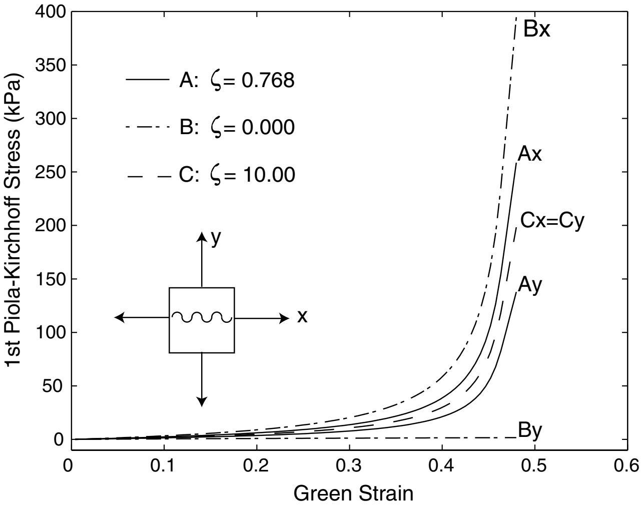

Fig. 7 The effect of splay on equibiaxial stress/strain response. All parameters were held fixed except for ς. The constants of condition A were the same as those used to obtain Fig. 6, condition B is the limiting case of transverse isotropy (i.e., no splay), while condition C is the limiting case of planar isotropy

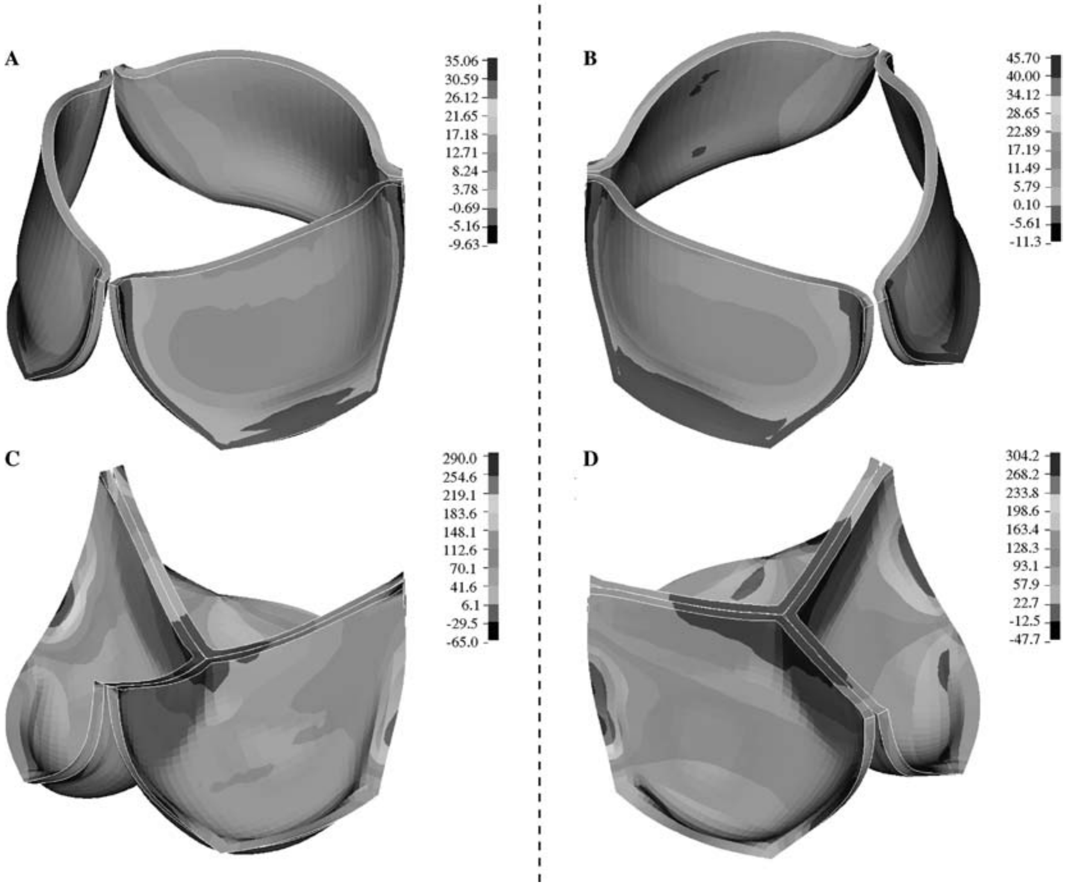
A
35.06
30.59
26.12
21.65
17.18
12.71
8.24
3.78
-0.69
-5.16
-9.63
B
45.70
40.00
34.12
28.65
22.89
17.19
11.49
5.79
0.10
-5.61
-11.3
C
290.0
254.6
219.1
183.6
148.1
112.6
70.1
41.6
6.1
-29.5
-65.0
D
304.2
268.2
233.8
198.6
163.4
128.3
93.1
57.9
22.7
-12.5
-47.7

Fig. 8 A comparison of two bioprosthetic valve simulations: one based on the invariant formulation (**A** , **B**), the other based on classical integrated splay (**C**, **D**). The invariant formulation was 2.65 times faster

8 Conclusion

We have proposed an efficient, invariant-based alternative to structural constitutive equations that accounts for a statistical dispersion of fibers. In contrast to existing models, our new invariant theory easily handles a 3D fiber population with a single mean preferred direction. The invariant theory is based on a novel closed-form 'splay invariant' that requires a single parameter in the 2D case, and two parameters in the 3D case. The proposed model fits biaxial data for aortic valve tissue better than existing aortic valve models. A modification in the fiber stress–strain law requires no reformulation of the constitutive tangent matrix, making the model flexible for different types of soft tissues. Most importantly, the model is computationally expedient in a finite-element analysis.

Acknowledgements The authors take this opportunity to thank Prof. Michael Sacks at the University of Pittsburgh for providing us with his experimental data, and to Dr. Todd Doehring at the Cleveland Clinic and Mr. Dimitri Deserranno at the National Center for Microgravity Research for many delightful discussions on this and related topics. Research partially funded by the US DOD via Award No. DAMD17-01-1-0673 to the Cleveland Clinic Foundation and Children's Hospital Los Angeles.

Appendices

The primary reason for adopting a Gaussian distribution to describe fiber splay is that the corresponding stiffness matrix κ can be computed analytically. Alternatively, Hurschler et al. (1997) have employed a von Mises distribution for splay in conjunction with a Weibull distribution for crimp that they collectively solve numerically.

1. A two-dimensional splay

We recall that our local coordinate system was chosen so that

$$[\![\mathbf{a}_0]\!]_i=\begin{Bmatrix}1\\0\\0\end{Bmatrix},\quad [\![\mathbf{e}_f]\!]_i=\begin{Bmatrix}\cos\theta\\ \sin\theta\\ 0\end{Bmatrix},\tag{46}$$

and as such

$$[\![\mathbf{e}_f\otimes\mathbf{e}_f]\!]_{ij}=\begin{bmatrix}\cos^2\theta & \sin\theta\cos\theta & 0\\ \sin\theta\cos\theta & \sin^2\theta & 0\\ 0 & 0 & 0\end{bmatrix},\tag{47}$$

which leads to an expression for Eq. 16 that can be solved analytically; it being,

$$[\![\kappa(\varsigma)]\!]_{ij}=\begin{bmatrix}\kappa_{11} & 0 & 0\\ 0 & \kappa_{22} & 0\\ 0 & 0 & 0\end{bmatrix},\tag{48}$$

where the two non-zero stiffness components have values of

$$\kappa_{11}=\frac{1}{2}+\frac{\mathrm{e}^{-2\varsigma^2}\left[\operatorname{erf}\left(\left(\pi+i4\varsigma^2\right)/2\sqrt{2}\varsigma\right)+\operatorname{erf}\left(\left(\pi-i4\varsigma^2\right)/2\sqrt{2}\varsigma\right)\right]}{4\operatorname{erf}\left(\pi/2\sqrt{2}\varsigma\right)},\tag{49}$$

and

$$\kappa_{22}=\frac{1}{2}-\frac{\mathrm{e}^{-2\varsigma^2}\left[\operatorname{erf}\left(\left(\pi+i4\varsigma^2\right)/2\sqrt{2}\varsigma\right)+\operatorname{erf}\left(\left(\pi-i4\varsigma^2\right)/2\sqrt{2}\varsigma\right)\right]}{4\operatorname{erf}\left(\pi/2\sqrt{2}\varsigma\right)},\tag{50}$$

wherein $i=\sqrt{-1}$ is the unit imaginary number. The sum of two error functions whose arguments are complex conjugates, i.e., $\operatorname{erf}(x+i\,y)+\operatorname{erf}(x-i\,y)$, produces a real result, and as such, κ_{11} and κ_{22} are both real numbers.

2. Three-dimensional splay

Here, the formulation is somewhat different; specifically,

$$[\![\mathbf{a}_0]\!]_i=\begin{Bmatrix}1\\0\\0\end{Bmatrix},\quad [\![\mathbf{e}_f]\!]_i=\begin{Bmatrix}\cos\theta\\ \sin\theta\cos\phi\\ \sin\theta\sin\phi\end{Bmatrix},\tag{51}$$

and as such

$$[\![\mathbf{e}_f\otimes\mathbf{e}_f]\!]_{ij}=\begin{bmatrix}\cos^2\theta & \sin\theta\cos\theta\cos\phi & \sin\theta\cos\theta\sin\phi\\ \sin\theta\cos\theta\cos\phi & \sin^2\theta\cos^2\phi & \sin^2\theta\sin\phi\cos\phi\\ \sin\theta\cos\theta\sin\phi & \sin^2\theta\sin\phi\cos\phi & \sin^2\theta\sin^2\phi\end{bmatrix},\tag{52}$$

which leads to an expression for Eq. 17 that can be solved analytically; it being,

$$[\![\boldsymbol{\kappa}(\varsigma)]\!]_{ij}=\begin{bmatrix}\kappa_{11} & 0 & 0\\ 0 & \kappa_{22} & 0\\ 0 & 0 & \kappa_{33}\end{bmatrix},\tag{53}$$

where the two non-zero stiffness components have values of

$$\kappa_{11}=\frac{1}{2}+\frac{\mathrm{e}^{-2\varsigma^2}\left[\operatorname{erf}\left(\left(\pi+i4\varsigma^2\right)/2\sqrt{2}\varsigma\right)+\operatorname{erf}\left(\left(\pi-i4\varsigma^2\right)/2\sqrt{2}\varsigma\right)\right]}{4\operatorname{erf}\left(\pi/2\sqrt{2}\varsigma\right)},\tag{54}$$

which is the same as Eq. 49, and

$$\kappa_{22} = \kappa_{33} = \frac{1}{4} - \frac{e^{-2\varsigma^2}\left[\operatorname{erf}\left(\left(\pi + i4\varsigma^2\right)/2\sqrt{2}\varsigma\right) + \operatorname{erf}\left(\left(\pi - i4\varsigma^2\right)/2\sqrt{2}\varsigma\right)\right]}{8\operatorname{erf}\left(\pi/2\sqrt{2}\varsigma\right)}, \tag{55}$$

where this value for κ_{22} is exactly half that of the 2D case (Eq. 50, wherein $\kappa_{33} = 0$) but here $\kappa_{33} = \kappa_{22}$.

3. Collagen model

A micro-structural model based on the physiology of crimped collagen fibers was recently derived by Freed and Doehring (2005) that we have altered to meet our needs (see Algorithm 1); specifically, given a fiber stretch λ, this model returns the engineering stress σ/λ and tangent modulus $\mathrm{d}\sigma/\mathrm{d}\lambda$ of the fiber. There are four physiological parameters (material constants defined at the top of the algorithm) that the user must supply; three if failure is not to be considered.

A typical pair of response curves are plotted in Fig. 9. The discontinuity observed in the $\mathrm{d}\sigma/\mathrm{d}\lambda$ curve indicates that the model presented in Algorithm 1 predicts a stress σ response that is continuous and differentiable in stretch λ up to fiber failure, which is not depicted in this figure. The values assigned to the model to obtain these curves were $H_0/r_0 = 27.5$, $R_0/r_0 = 2$, and $E_f = 45$ MPa, which results in a transitional stretch Λ of 1.1. This is but one example of a fiber stress/stretch model.

Algorithm 1

Given H_0/r_0, E_f *and* λ_u, *where* H_0 *is the initial wavelength of crimp,* R_0 *is the initial amplitude of crimp,* r_0 *is the initial fibril radius,* E_f *is the elastic modulus of the fiber in the linear region, and* λ_u *is its ultimate stretch, then:*

Set $r_0 = 1$ *so that* $H_0 \equiv H_0/r_0$ & $R_0 \equiv R_0/r_0$

Compute the constant parameters: $L_0 = \left((2\pi R_0)^2 + H_0^2\right)^{1/2}$, $\Lambda = L_0/H_0 < \lambda_u$, $E_s = E_f H_0/\{H_0 + [1 + 37/6\pi^2 + 2(L_0/\pi r_0)^2](L_0 - H_0)\}$, *where* L_0 *is the chord length of helix over one wavelength, while* Λ *is the stretch and* E_s *is the secant modulus at the transition between the toe and linear regions.*

If $\lambda \leq \Lambda$ *Then*

$$\xi = 6(\pi r_0)^2[\Lambda^2 + (4\pi^2 - 1)\lambda^2]\lambda/\{\Lambda\{3H_0^2(\Lambda^2 - \lambda^2)[3\Lambda^2 + (8\pi^2 - 3)\lambda^2] + 8(\pi r_0)^2[10\Lambda^2 + (3\pi^2 - 10)\lambda^2]\}\},$$

$$\begin{aligned}\mathrm{d}\xi/\mathrm{d}\lambda = \{&18H_0^2(\pi r_0)^2[3\Lambda^6 + (28\pi^2 - 3)\Lambda^4\lambda^2 \\ &+ (32\pi^4 - 8\pi^2 - 3)\Lambda^2\lambda^4 + (32\pi^4 - 20\pi^2 + 3)\lambda^6] \\ &+ 48(\pi r_0)^4[10\Lambda^4 + (117\pi^2 - 20)\Lambda^2\lambda^2 + (12\pi^4 \\ &- 43\pi^2 + 10)\lambda^4]\}/\{\Lambda\{3H_0^2(\Lambda^2 - \lambda^2)[3\Lambda^2 \\ &+ (8\pi^2 - 3)\lambda^2] + 8(\pi r_0)^2[10\Lambda^2 + (3\pi^2 - 10)\lambda^2]\}^2\},\end{aligned}$$

$\sigma/\lambda = \xi E_s(\lambda - 1)/\lambda$ &

$\mathrm{d}\sigma/\mathrm{d}\lambda = E_s[\xi + (\lambda - 1)\mathrm{d}\xi/\mathrm{d}\lambda]$

Else If $\Lambda \leq \lambda \leq \lambda_u$ *Then*

$\sigma/\lambda = E_s(\Lambda - 1)/\lambda + E_f(\lambda - \Lambda)/\lambda$ & $\mathrm{d}\sigma/\mathrm{d}\lambda = E_f$

Else Fibril Failure

$\sigma/\lambda = 0$ & $\mathrm{d}\sigma/\mathrm{d}\lambda = 0.$

Return σ/λ and $\mathrm{d}\sigma/\mathrm{d}\lambda$.

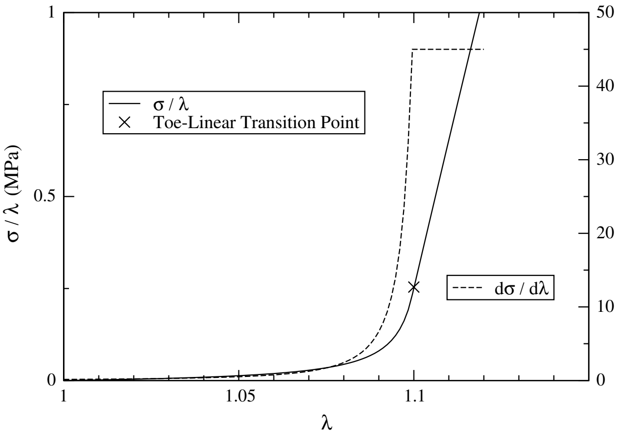

Fig. 9 Typical soft-tissue response curves for σ / λ and $\mathrm{d}\sigma$ / $\mathrm{d}\lambda$

4. Voigt notation for dyadic products of tensors

Because the Lagrangian fields for stress S_{ij} and strain E_{ij}, $i,j = 1,2,3$, are symmetric tensors, it is customary to express their components as six-dimensional arrays S_α and E_α, $\alpha = 1,2,\ldots,6$ (Belytschko et al. 2000, pp 615–618). These arrays are not vector fields in the sense that they do not obey the tensor-transformation law; nevertheless, they have proven to be very useful in the employ of finite elements.

A linear approximation for stress increment d S_{ij} relates to the strain increment $\mathrm{d}E_{ij} = \frac{1}{2}\mathrm{d}C_{ij}$ in the Lagrangian frame through

$$\mathrm{d}S_{ij} = \mathbb{C}_{ijk\ell}\mathrm{d}E_{k\ell} \quad \text{with} \quad \mathbb{C}_{ijk\ell} = \frac{\partial S_{ij}}{\partial E_{k\ell}}$$

$$\therefore \quad \mathrm{d}S_\alpha = \mathbb{C}_{\alpha\beta}\mathrm{d}E_\beta, \tag{56}$$

where the tangent modulus $\mathbb{C}$ has a Voigt representation of

$$[[\mathbb{C}]]_{\alpha\beta}=\begin{bmatrix} \mathbb{C}_{11} & \mathbb{C}_{12} & \mathbb{C}_{13} & \mathbb{C}_{14} & \mathbb{C}_{15} & \mathbb{C}_{16} \\ \mathbb{C}_{21} & \mathbb{C}_{22} & \mathbb{C}_{23} & \mathbb{C}_{24} & \mathbb{C}_{25} & \mathbb{C}_{26} \\ \mathbb{C}_{31} & \mathbb{C}_{32} & \mathbb{C}_{33} & \mathbb{C}_{34} & \mathbb{C}_{35} & \mathbb{C}_{36} \\ \mathbb{C}_{41} & \mathbb{C}_{42} & \mathbb{C}_{43} & \mathbb{C}_{44} & \mathbb{C}_{45} & \mathbb{C}_{46} \\ \mathbb{C}_{51} & \mathbb{C}_{52} & \mathbb{C}_{53} & \mathbb{C}_{54} & \mathbb{C}_{55} & \mathbb{C}_{56} \\ \mathbb{C}_{61} & \mathbb{C}_{62} & \mathbb{C}_{63} & \mathbb{C}_{64} & \mathbb{C}_{65} & \mathbb{C}_{66} \end{bmatrix}$$
$$=\begin{bmatrix} \mathbb{C}_{1111} & \mathbb{C}_{1122} & \mathbb{C}_{1133} & \mathbb{C}_{1112} & \mathbb{C}_{1113} & \mathbb{C}_{1123} \\ \mathbb{C}_{2211} & \mathbb{C}_{2222} & \mathbb{C}_{2233} & \mathbb{C}_{2212} & \mathbb{C}_{2213} & \mathbb{C}_{2223} \\ \mathbb{C}_{3311} & \mathbb{C}_{3322} & \mathbb{C}_{3333} & \mathbb{C}_{3312} & \mathbb{C}_{3313} & \mathbb{C}_{3323} \\ \mathbb{C}_{1211} & \mathbb{C}_{1222} & \mathbb{C}_{1233} & \mathbb{C}_{1212} & \mathbb{C}_{1213} & \mathbb{C}_{1223} \\ \mathbb{C}_{1311} & \mathbb{C}_{1322} & \mathbb{C}_{1333} & \mathbb{C}_{1312} & \mathbb{C}_{1313} & \mathbb{C}_{1323} \\ \mathbb{C}_{2311} & \mathbb{C}_{2322} & \mathbb{C}_{2333} & \mathbb{C}_{2312} & \mathbb{C}_{2313} & \mathbb{C}_{2323} \end{bmatrix}, \tag{57}$$

with $\mathbb{C}_{\alpha\beta} \neq \mathbb{C}_{\beta\alpha}$ unless the $\mathbb{C}_{ijk\ell}$ possess major symmetry $\mathbb{C}_{ijk\ell}=\mathbb{C}_{k\ell ij}$. The tangent modulus always possesses minor symmetries $\mathbb{C}_{ijk\ell}=\mathbb{C}_{ij\ell k}=\mathbb{C}_{jik\ell}=\mathbb{C}_{ji\ell k}$ because of the inherent symmetries in S_{ij} and C_{ij}. Major symmetry follows automatically if stress S_{ij} is given by some potential function F such that $S_{ij}=\partial F/\partial E_{ij}$,as in hyperelasticity.

Three dyadic products of tensor fields arise naturally when deriving tangent moduli, in the sense of Eqs. D1 and D2. Of these three, there are two fundamental dyadic products that we denote as $\mathrm{A} \otimes \mathrm{B}$ and $\mathrm{A} \boxtimes \mathrm{B}$; we call them the outer- and inner-dyadic products, respectively, or the circle- and box-products for short, wherein A and B are taken to be symmetric fields. The third dyadic product, denoted as $\mathrm{A} \odot \mathrm{A}$, is a special case of the inner-dyadic product $\mathrm{A} \boxtimes \mathrm{A}$ wherein both arguments are the same tensor field—in this case, A. We know of no publication where $\mathrm{A}\boxtimes\mathrm{B}$ has been defined as we use it, which is the main reason for writing this appendix.

The circle product $\mathrm{A} \otimes \mathrm{B}$ is well known and has components

$$\begin{aligned}(\mathrm{A} \otimes \mathrm{B})_{ijk\ell} &= \frac{1}{4}\left(A_{ij}B_{k\ell} + A_{ij}B_{\ell k} + A_{ji}B_{k\ell} + A_{ji}B_{\ell k}\right) \\ &\equiv A_{ij}B_{k\ell},\end{aligned} \tag{58}$$

which reduce down to the simple expression $(\mathrm{A} \otimes \mathrm{B})_{ijk\ell} = A_{ij}B_{k\ell}$ as a consequence of A and B being symmetric. This dyadic product has the simple Voigt notation of

$$[[\mathrm{A} \otimes \mathrm{B}]]_{\alpha\beta} = \begin{bmatrix} A_{11}B_{11} & A_{11}B_{22} & A_{11}B_{33} & A_{11}B_{12} & A_{11}B_{13} & A_{11}B_{23} \\ A_{22}B_{11} & A_{22}B_{22} & A_{22}B_{33} & A_{22}B_{12} & A_{22}B_{13} & A_{22}B_{23} \\ A_{33}B_{11} & A_{33}B_{22} & A_{33}B_{33} & A_{33}B_{12} & A_{33}B_{13} & A_{33}B_{23} \\ A_{12}B_{11} & A_{12}B_{22} & A_{12}B_{33} & A_{12}B_{12} & A_{12}B_{13} & A_{12}B_{23} \\ A_{13}B_{11} & A_{13}B_{22} & A_{13}B_{33} & A_{13}B_{12} & A_{13}B_{13} & A_{13}B_{23} \\ A_{23}B_{11} & A_{23}B_{22} & A_{23}B_{33} & A_{23}B_{12} & A_{23}B_{13} & A_{23}B_{23} \end{bmatrix}. \tag{59}$$

Matrix $(\mathrm{A} \otimes \mathrm{B})_{\alpha\beta}$ is not symmetric unless $\mathrm{A} = \mathrm{B}$; however, $(\mathrm{A} \otimes \mathrm{B}) + (\mathrm{B} \otimes \mathrm{A})$ does yield a symmetric matrix in Voigt notation. This is because $\mathrm{A} \otimes \mathrm{B}$ possesses minor symmetry, but not major symmetry, therefore $(\mathrm{A} \otimes \mathrm{B})_{\alpha\beta} \neq (\mathrm{A} \otimes \mathrm{B})_{\beta\alpha}$, in general. The box product $\mathrm{A} \boxtimes \mathrm{B}$ is a new dyadic product that we define by the sum

$$(\mathrm{A} \boxtimes \mathrm{B})_{ijk\ell} = \frac{1}{4}\left(A_{ik}B_{j\ell} + A_{i\ell}B_{jk} + A_{jk}B_{i\ell} + A_{j\ell}B_{ik}\right), \tag{60}$$

and possesses minor and major symmetries, therefore $(\mathrm{A} \boxtimes \mathrm{B})_{\alpha\beta} = (\mathrm{A} \boxtimes \mathrm{B})_{\beta\alpha}$; consequently, the box product commutes, viz., $\mathrm{A} \boxtimes \mathrm{B} = \mathrm{B} \boxtimes \mathrm{A}$. A special case that arises frequently in practice is when both tensor arguments of this product are the same. This dyadic product is well known and has its own notation of $\mathrm{A} \odot \mathrm{A}$ (cf., Holzapfel (2000, pg. 254)) with components

$$(\mathrm{A} \odot \mathrm{A})_{ijk\ell} = \frac{1}{2}\left(A_{ik}A_{j\ell} + A_{i\ell}A_{jk}\right). \tag{61}$$

The Voigt representation of $(\mathrm{A} \boxtimes \mathrm{B})_{\alpha\beta}$ has the following symmetric matrix components:

$$\begin{cases} (\mathrm{A} \boxtimes \mathrm{B})_{11} = A_{11}B_{11}, \\ (\mathrm{A} \boxtimes \mathrm{B})_{12} = A_{12}B_{12}, \\ (\mathrm{A} \boxtimes \mathrm{B})_{13} = A_{13}B_{13}, \\ (\mathrm{A} \boxtimes \mathrm{B})_{14} = \frac{1}{2}\left(A_{11}B_{12} + A_{12}B_{11}\right), \\ (\mathrm{A} \boxtimes \mathrm{B})_{15} = \frac{1}{2}\left(A_{11}B_{13} + A_{13}B_{11}\right), \\ (\mathrm{A} \boxtimes \mathrm{B})_{16} = \frac{1}{2}\left(A_{12}B_{13} + A_{13}B_{12}\right), \\ (\mathrm{A} \boxtimes \mathrm{B})_{22} = A_{22}B_{22}, \\ (\mathrm{A} \boxtimes \mathrm{B})_{23} = A_{23}B_{23}, \\ (\mathrm{A} \boxtimes \mathrm{B})_{24} = \frac{1}{2}\left(A_{12}B_{22} + A_{22}B_{12}\right), \\ (\mathrm{A} \boxtimes \mathrm{B})_{25} = \frac{1}{2}\left(A_{12}B_{23} + A_{23}B_{12}\right), \\ (\mathrm{A} \boxtimes \mathrm{B})_{26} = \frac{1}{2}\left(A_{22}B_{23} + A_{23}B_{22}\right), \\ (\mathrm{A} \boxtimes \mathrm{B})_{33} = A_{33}B_{33}, \\ (\mathrm{A} \boxtimes \mathrm{B})_{34} = \frac{1}{2}\left(A_{13}B_{23} + A_{23}B_{13}\right), \\ (\mathrm{A} \boxtimes \mathrm{B})_{35} = \frac{1}{2}\left(A_{13}B_{33} + A_{33}B_{13}\right), \\ (\mathrm{A} \boxtimes \mathrm{B})_{36} = \frac{1}{2}\left(A_{23}B_{33} + A_{33}B_{23}\right), \\ (\mathrm{A} \boxtimes \mathrm{B})_{44} = \frac{1}{4}\left(A_{11}B_{22} + 2A_{12}B_{12} + A_{22}B_{11}\right), \\ (\mathrm{A}\boxtimes\mathrm{B})_{45} = \frac{1}{4}\left(A_{11}B_{23} + A_{13}B_{12} + A_{12}B_{13} + A_{23}B_{11}\right), \\ (\mathrm{A}\boxtimes\mathrm{B})_{46} = \frac{1}{4}\left(A_{12}B_{23} + A_{13}B_{22} + A_{22}B_{13} + A_{23}B_{12}\right), \\ (\mathrm{A}\boxtimes\mathrm{B})_{55} = \frac{1}{4}\left(A_{11}B_{33} + 2A_{13}B_{13} + A_{33}B_{11}\right), \\ (\mathrm{A}\boxtimes\mathrm{B})_{56} = \frac{1}{4}\left(A_{12}B_{33} + A_{13}B_{23} + A_{23}B_{13} + A_{33}B_{12}\right), \\ (\mathrm{A}\boxtimes\mathrm{B})_{66} = \frac{1}{4}\left(A_{22}B_{33} + 2A_{23}B_{23} + A_{33}B_{22}\right) \end{cases} \tag{62}$$

while the Voigt representation of $(\mathrm{A} \odot \mathrm{A})_{\alpha\beta}$ has symmetric matrix components:

$$\begin{cases} (\mathrm{A} \odot \mathrm{A})_{11} = A_{11}^2, \\ (\mathrm{A} \odot \mathrm{A})_{12} = A_{12}^2, \\ (\mathrm{A} \odot \mathrm{A})_{13} = A_{13}^2, \\ (\mathrm{A} \odot \mathrm{A})_{14} = A_{11}A_{12}, \\ (\mathrm{A} \odot \mathrm{A})_{15} = A_{11}A_{13}, \\ (\mathrm{A} \odot \mathrm{A})_{16} = A_{12}A_{13}, \\ (\mathrm{A} \odot \mathrm{A})_{22} = A_{22}^2, \\ (\mathrm{A} \odot \mathrm{A})_{23} = A_{23}^2, \\ (\mathrm{A} \odot \mathrm{A})_{24} = A_{12}A_{22}, \\ (\mathrm{A} \odot \mathrm{A})_{25} = A_{12}A_{23}, \\ (\mathrm{A} \odot \mathrm{A})_{26} = A_{22}A_{23}, \\ (\mathrm{A} \odot \mathrm{A})_{33} = A_{33}^2, \\ (\mathrm{A} \odot \mathrm{A})_{34} = A_{13}A_{23}, \\ (\mathrm{A} \odot \mathrm{A})_{35} = A_{13}A_{33}, \\ (\mathrm{A} \odot \mathrm{A})_{36} = A_{23}A_{33}, \\ (\mathrm{A} \odot \mathrm{A})_{44} = \frac{1}{2}\left(A_{11}A_{22} + A_{12}^2\right), \\ (\mathrm{A} \odot \mathrm{A})_{45} = \frac{1}{2}\left(A_{11}A_{23} + A_{13}A_{12}\right), \\ (\mathrm{A} \odot \mathrm{A})_{46} = \frac{1}{2}\left(A_{12}A_{23} + A_{13}A_{22}\right), \\ (\mathrm{A} \odot \mathrm{A})_{55} = \frac{1}{2}\left(A_{11}A_{33} + A_{13}^2\right), \\ (\mathrm{A} \odot \mathrm{A})_{56} = \frac{1}{2}\left(A_{12}A_{33} + A_{13}A_{23}\right), \\ (\mathrm{A} \odot \mathrm{A})_{66} = \frac{1}{2}\left(A_{22}A_{33} + A_{23}^2\right), \end{cases} \tag{63}$$

wherein terms on the right-hand side are tensor components while those on the left-hand side are the Voigt components. Obviously, $\odot$ and $\boxtimes$ are different products.

Example

The theory of linear elasticity has stress components

$$\begin{cases} S_1 = S_{11} = \lambda(E_1 + E_2 + E_3) + 2\mu E_1, \\ S_2 = S_{22} = \lambda(E_1 + E_2 + E_3) + 2\mu E_2, \\ S_3 = S_{33} = \lambda(E_1 + E_2 + E_3) + 2\mu E_3, \\ S_4 = S_{12} = \mu E_4, \\ S_5 = S_{13} = \mu E_5, \\ S_6 = S_{23} = \mu E_6, \end{cases}$$

where

$$\begin{cases} E_1 = E_{11}, \\ E_2 = E_{22}, \\ E_3 = E_{33}, \\ E_4 = 2E_{12}, \\ E_5 = 2E_{13}, \\ E_6 = 2E_{23}, \end{cases}$$

and as such, its tangent modulus is readily determined to be

$$(\mathbb{C})_{\alpha\beta} = \lambda(\mathrm{I} \otimes \mathrm{I})_{\alpha\beta} + 2\mu(\mathrm{I} \odot \mathrm{I})_{\alpha\beta},$$

wherein λ and μ are the elastic moduli, and where

$$[[\mathrm{I}]]_\alpha = \begin{Bmatrix} 1 \\ 1 \\ 1 \\ 0 \\ 0 \\ 0 \end{Bmatrix}, \quad [[\mathrm{I} \otimes \mathrm{I}]]_{\alpha\beta} = \left\{\begin{matrix} 1 & 1 & 1 & 0 & 0 & 0 \\ 1 & 1 & 1 & 0 & 0 & 0 \\ 1 & 1 & 1 & 0 & 0 & 0 \\ 0 & 0 & 0 & 0 & 0 & 0 \\ 0 & 0 & 0 & 0 & 0 & 0 \\ 0 & 0 & 0 & 0 & 0 & 0 \end{matrix}\right],$$

$$[[\mathrm{I} \odot \mathrm{I}]]_{\alpha\beta} = \left\{\begin{matrix} 1 & 0 & 0 & 0 & 0 & 0 \\ 0 & 1 & 0 & 0 & 0 & 0 \\ 0 & 0 & 1 & 0 & 0 & 0 \\ 0 & 0 & 0 & 1/2 & 0 & 0 \\ 0 & 0 & 0 & 0 & 1/2 & 0 \\ 0 & 0 & 0 & 0 & 0 & 1/2 \end{matrix}\right]$$

The $\frac{1}{2}$'s in $(\mathrm{I} \odot \mathrm{I})_{\alpha\beta}$ are offset by the 2's present in E_β.

References

Belytschko T, Liu WK, Moran B (2000) Nonlinear finite elements for continua and structures. Wiley, Chichester

Billiar KL, Sacks MS (2000a) Biaxial mechanical properties of the natural and glutaraldehyde-treated aortic valve cusp—Part I: experimental results. ASME J Biomech Eng 122:23–30

Billiar KL, Sacks MS (2000b) Biaxial mechanical properties of the natural and glutaraldehyde-treated aortic valve cusp—Part II: a structural constitutive model. ASME J Biomech Eng 122:327–335

Cauchy A-L (1827) Exercices de Mathématiques, vol 2. de Bure Frères, Paris

Criscione JC, Douglas AS, Hunter WC (2001) Physically based strain invariant set for materials exhibiting transversely isotropic behavior. J Mech Phys Solids 49:871–897

Doehring TC, Carew EO, Vesely I (2004) The effect of strain rate on the viscoelastic response of aortic valve tissue: a direct-fit approach. Ann Biomed Eng 32:223–232

Einstein DR (2002) Nonlinear acoustic analysis of the mitral valve. PhD thesis, University of Washington, Seattle

Finger J (1894) Über die allgemeinsten Beziehungen zwischen endlichen Deformationen und den zugehörigen Spannungen in aeolotropen und isotropen Substanzen. Sitzungsberichte der Akademie der Wissenschaften Wien 103:1073–1100

Flory PJ (1961) Thermodynamic relations for high elastic materials. Trans Faraday Soc 57:829–838

Freed AD, (2004) Transverse-isotropic elastic and viscoelastic solids. ASME J Eng Mater Technol 126:38–44

Freed AD, Doehring TC (2005) Elastic model for crimped collagen fibrils. ASME J Biomech Eng (in press)

Green G (1841) On the propagation of light in crystallized media. Trans Cambridge Phil Soc 7:121–140

Hartmann S, Neff P (2003) Polyconvexity of generalized polynomial-type hyperelastic strain energy functions for near-incompressibility. Int J Solids Struct 40:2767–2791

Hencky H (1928) Über die Form des Elastizitätsgesetzes bei ideal elastischen Stoffen. Z Tech Phys 9:215–220

Holzapfel GA (2000) Nonlinear solid mechanics: a continuum approach for engineering. Wiley, Chichester

Holzapfel GA, Gasser TC, Stadler M (2002) A structural model for the viscoelastic behavior of arterial walls: continuum formulation and finite element analysis. Eur J Mech A Solids 21:441–463

Holzapfel GA, Weizsäcker HW (1998) Biomechanical behavior of the arterial wall and its numerical characterization. Comput Biol Med 28:377–392

Horowitz A, Lanir Y, Yin FC, Perl M, Sheinman I, Strumpf RK (1988) Structural three-dimensional constitutive law for the passive myocardium. ASME J Biomech Eng 110:200–207

Hurschler C, Loitz-Ramage B, Vanderby R Jr (1997) A structurally based stress-stretch relationship for tendon and ligament. ASME J Biomech Eng 119:392–399

Lanir Y (1983) Constitutive equations for fibrous connective tissues. J Biomech 16:1–12

Leonov AI (2000) On the conditions of potentiality in finite elasticity and hypo-elasticity. Int J Solids Struct 37:2565–2576

Lodge AS (1974) Body tensor fields in continuum mechanics: with applications to polymer rheology. Academic, New York

Malkus DS, Hughes TJR (1978) Mixed finite element methods—reduced and selective integration techniques: a unification of concepts. Comput Meth Appl Mech Eng 15:63–81

Mijailovich A, Stamenovic D, Fredberg JJ (1993) Toward a kinetic theory of connective tissue micromechanics. J Appl Physiol 74:665–681

Mooney M (1940) A theory of large elastic deformations. J Appl Phys 11:582–592

Sacks MS (2000) Biaxial mechanical evaluation of planar biological materials. J Elasticity 61:199–246

Sacks MS (2003) Incorporation of experimentally-derived fiber orientation into a structural consitutive model for planar collagenous tissues. ASME J Biomech Eng 125:280–287

Simo JC, Hughes TJR (1998) Computational inelasticity, vol 7 of Interdisiplinary applied mathematics. Springer, Berlin Heidelberg New York

Simo JC, Taylor RL (1991) Quasi-incompressible finite elasticity in principal stretches. Continuum basis and numerical algorithms. Comp Meth Appl Mech Eng 85:273–310

Spencer AJM (1972) Deformations of fibre-reinforced materials. Clarendon, Oxford

Sussman T, Bathe K-J (1987) A finite element formulation for nonlinear incompressible elastic and inelastic analysis. Comput Struct 26:357–409

Wuyts FL, Vanhuyse VJ, Langewouters GJ, Decraemer WF, Raman ER, Buyle S (1995) Elastic properties of human aortas in relation to age and atherosclerosis: a structural model. Phys Med Biol 40:1577–1597

Zioupos P, Barbenel JC (1994) Mechanics of native bovine pericardium: I. The multiangular behavior of strength and stiffness of the tissue. Biomaterials 15:366–373